

# Impact of cosmic web on galaxy properties and their correlations: Insights from Principal Component Analysis

Anindita Nandi<sup>a</sup>, Biswajit Pandey<sup>a</sup>

<sup>a</sup>*Department of Physics, Visva-Bharati University, , Santiniketan, 731235, West Bengal, India*

---

## Abstract

We use Principal Component Analysis (PCA) to analyze a volume-limited sample from the SDSS and explore how cosmic web environments affect the interrelations between various galaxy properties, such as  $(u - r)$  colour, stellar mass, specific star formation rate, metallicity, morphology, and  $D4000$ . Our analysis reveals that the first three principal components (PC1, PC2 and PC3) account for approximately  $\sim 85\%$  of the data variance. We classify galaxies into different cosmic web environments based on the eigenvalues of the deformation tensor and compare PC1, PC2, PC3 across these environments, ensuring a mass-matched sample of equal size for each environment. PC1 is dominated by colour, sSFR,  $D4000$ , and morphology. It displays clear bimodality across all cosmic web environments, with sheets and clusters showing distinct preferences for negative and positive PC1 values, respectively. This variation reflects the strong role of environmental processes in regulating star formation. PC2 and PC3, respectively show positively and negatively skewed unimodal distributions in all environments. PC2 is primarily influenced by metallicity whereas PC3 is dominated by stellar mass. It indicates that metallicity evolves gradually and is less sensitive to environmental extremes, highlighting the importance of internal, secular processes. PC3 likely captures residual variation in stellar mass within the two main galaxy populations (star-forming and quiescent) separated by PC1. A Kolmogorov-Smirnov (KS) test confirms that the distributions of PC1, PC2 and PC3 differ significantly across environments, with a confidence level exceeding 99.99%. Furthermore, we calculate the normalized mutual information (NMI) between the principal components and individual galaxy properties within different cosmic web environments. A two-tailed t-test reveals that for each relationship and each pair of environments, the null hypothesis is rejected with a confidence level  $> 99.99\%$ . Our analysis confirms that cosmic web environments play a significant role in shaping the correlations between galaxy properties.

**Keywords:** cosmology; large-scale structure of Universe; galaxies; statistics; methods: data analysis

---

## 1. Introduction

The origin and evolution of galaxies stands as a paramount challenge in modern cosmology. It remains at the forefront of research in cosmology over recent decades. According to the current paradigm, the first bound structures emerge from the collapse of initial fluctuations into dark matter halos. These halos accumulate neutral hydrogen gas from their surroundings via accretion, which eventually condenses and cools, forming galaxies at their cores (Rees and Ostriker, 1977; Silk, 1977; White and Rees, 1978; Fall and Efstathiou, 1980). In this narrative, the primary mechanism driving galaxy growth is the accretion of gas from the intergalactic medium (IGM). As galaxies evolve, the formation of a supermassive black hole at their centers and the efficient accretion onto it can ignite active galactic nuclei (AGN) activity. The feedback from the energetic processes like AGN, supernovae or shock-driven winds can drive gas outflows from galaxies. The expelled gas cools over time and reenters the galaxy, perpetuating the cycle.

The gas inflow and outflow can modulate the galaxy properties. Gas inflow supplies the raw fuel for star formation. It can trigger bursts of star formation, influencing the mass, colour and morphology of galaxies. The inflowing gas also brings pristine material into galaxies, which affects their chemical composition. Conversely, outflows can regulate

---

*Email addresses:* anindita.nandi96@gmail.com (Anindita Nandi), biswap@visva-bharati.ac.in (Biswajit Pandey)

star formation by ejecting gas from the galaxy, thereby reducing the available gas reservoir. Strong outflows can even lead to the quenching of star formation in galaxies. Moreover, outflows transport the heavy elements synthesized in stars into the interstellar medium (ISM) and IGM leading to metal enrichment of the gas over cosmic time.

It is also crucial to remember that galaxies do not evolve in isolation. The interaction of galaxies with their environment plays a very important role in their evolution. The influence of environment on shaping galaxy properties has been thoroughly explored in the literature (Davis and Geller, 1976; Dressler, 1980; Butcher and Oemler, 1984; Guzzo et al., 1997; Zehavi et al., 2002; Goto et al., 2003; Hogg et al., 2003; Blanton et al., 2003; Einasto et al., 2003; Balogh et al., 2002; Kauffmann et al., 2004; Mandelbaum et al., 2006; Abbas and Sheth, 2006; Pandey and Bharadwaj, 2007; Mouhcine et al., 2007; Bamford et al., 2009; Cooper et al., 2010; Koyama et al., 2013). Numerous studies using simulations (Toomre and Toomre, 1972; Barnes and Hernquist, 1996; Mihos and Hernquist, 1996; Tissera et al., 2002; Cox et al., 2006; Montuori et al., 2010; Lotz et al., 2011; Torrey et al., 2012; Hopkins et al., 2013; Renaud et al., 2014, 2015; Moreno et al., 2015, 2021; Renaud et al., 2022; Das and Pandey, 2024) and observations (Larson and Tinsley, 1978; Barton et al., 2000; Lambas et al., 2003; Alonso et al., 2004; Nikolic et al., 2004; Woods et al., 2006; Woods and Geller, 2007; Barton et al., 2007; Ellison et al., 2008; Ellison et al., 2010; Woods et al., 2010; Patton et al., 2011; Barrera-Ballesteros et al., 2015; Thorp et al., 2022; Shah et al., 2022; Das et al., 2023) have confirmed that tidal torques resulting from galaxy interactions can trigger starbursts and modify the colour and morphology of galaxies. Further, feedback mechanisms are not the sole drivers of gas outflows and quenching in galaxies. Several environment driven mechanisms such as merger (Hopkins et al., 2008), harassment (Moore et al., 1996, 1998), strangulation (Gunn and Gott, 1972; Balogh et al., 2000), starvation (Larson et al., 1980; Somerville and Primack, 1999; Kawata and Mulchaey, 2008) and satellite quenching (Geha et al., 2012) can shut down star formation in galaxies and alter their structures. Additional routes that can halt star formation in galaxies include mass quenching (Birnboim and Dekel, 2003; Dekel and Birnboim, 2006; Kereš et al., 2005; Gabor et al., 2010), morphological quenching (Martig et al., 2009), bar quenching (Masters et al., 2010) and angular momentum quenching (Peng and Renzini, 2020).

The environment of a galaxy is primarily characterized by the local density. Most earlier studies investigating the impact of environment on galaxy evolution have utilized local density as a proxy measure for assessing environmental influences. However, galaxies are organized into a complex interconnected structure of filaments, clusters, sheets, and voids known as the cosmic web (Gregory and Thompson, 1978; Jöeveer and Einasto, 1978; Einasto et al., 1980; Zeldovich and Shandarin, 1982; Einasto et al., 1984; Bond et al., 1996; Bharadwaj et al., 2000; Pandey and Bharadwaj, 2005; Aragón-Calvo et al., 2010; Libeskind et al., 2017), indicating that their environment cannot be fully characterized by local density alone. The cosmic web acts as a scaffolding that organizes and shapes the distribution of matter and galaxies on cosmic scales. Studies with N-body simulations reveal a dynamic flow of matter through the cosmic web: from voids to walls, walls to filaments, and ultimately into clusters (Aragón-Calvo et al., 2010; Cautun et al., 2014; Ramachandra and Shandarin, 2015; Wang et al., 2024). Moreover, hydrodynamical simulations suggest that more than (40–50)% baryonic matter resides in filaments as the Warm-Hot Intergalactic Medium (WHIM) which can profoundly impact the efficiency of gas accretion onto galaxies (Tuominen et al., 2021; Galárraga-Espinosa et al., 2021). The galaxies residing in different cosmic web environment may have different gas accretion efficiency (Cornuault et al., 2016; Zhu et al., 2022). Galaxies located near the centres of cosmic filaments and sheets benefit from a consistent influx of cold gas, fueling vigorous star formation and boosting their overall mass (Chen et al., 2017a; Pandey and Sarkar, 2020; Singh et al., 2020; Laigle et al., 2015; Das et al., 2023; Das et al., 2023; Hoosain et al., 2024). A recent study (Bulichi et al., 2024) using the SIMBA simulation (Davé et al., 2019) suggests that shock heating in filaments can also suppress star formation. Another study (Hasan et al., 2024) utilizing the IllustrisTNG simulation (Nelson et al., 2019) indicates that satellite galaxies are significantly more susceptible to such quenching within the filaments. Clusters are the most densely populated regions within the cosmic web, typically forming at the intersections of filaments. The galaxies in such environment experience heightened gas accretion rates and increased interactions with neighboring galaxies, the cluster potential, and the gas (Treu et al., 2003; De Lucia et al., 2012), often leading to intense bursts of star formation and structural changes. Recent studies suggest that galaxies located nearer to clusters show higher gas-phase metallicity independent of stellar mass and overdensity, indicating enhanced chemical enrichment compared to galaxies farther away (Donnan et al., 2022). In contrast, galaxies residing in the sparser regions and voids tend to undergo quieter evolutionary paths, marked by more subdued star formation activities (Einasto et al., 2022; Rodríguez-Medrano et al., 2024). This intricate interplay within the cosmic web underscores its pivotal role in shaping the diverse trajectories of galaxy evolution across the universe.

Several studies (Zehavi et al., 2011; Yan et al., 2013; Alpaslan et al., 2015; Alam et al., 2019) do not detect a

significant impact of tidal environments on galaxy properties, attributing observed differences to variations in the underlying halo mass function within the cosmic web or the assembly history of dark matter halos. In recent years, observational evidence has increasingly shown that galaxy properties are also influenced by their large-scale environment (Pandey and Bharadwaj, 2006, 2008; Trujillo et al., 2006; Lee and Erdogdu, 2007; Paz et al., 2008; Jones et al., 2010; Scudder et al., 2012; Tempel and Libeskind, 2013; Tempel et al., 2013; Darvish et al., 2014; Filho et al., 2015; Luparello et al., 2015; Alpaslan et al., 2016; Pandey and Sarkar, 2017; Kuutma et al., 2017; Chen et al., 2017b; Lee, 2018; Laigle et al., 2018; Kraljic et al., 2018; Chen et al., 2019; Pandey and Sarkar, 2020; Kraljic et al., 2020; Bonjean et al., 2020; Winkel et al., 2021; Malavasi et al., 2022; Bhambhani et al., 2023). Galaxy properties such as stellar mass, colour, morphology, star formation rate, star formation history, and metallicity are correlated with each other, and these connections might change depending on the cosmic web environment. The influence of various morphological environments within the cosmic web on shaping the correlations among galaxy properties remains relatively unclear. A recent study (Nandi et al., 2024) use Pearson Correlation Coefficient (PCC) and Normalized Mutual Information (NMI) to analyze the correlations between galaxy properties in different environments of the cosmic web. The study demonstrates that the scaling relations between observable galaxy properties are influenced by the geometric environments of the cosmic web. In the present work, we will use Principal Component Analysis (PCA) (Pearson, 1901) to analyze data from the Sloan Digital Sky Survey (SDSS). The Sloan Digital Sky Survey (SDSS) (Stoughton et al., 2002) stands as one of the largest galaxy redshift surveys conducted to date. The availability of precise photometric and spectroscopic information for a large number of galaxies in the SDSS has enabled accurate measurement of their physical properties. This rich data provides an excellent opportunity for analyzing the impact of the cosmic web on the correlations between various galaxy properties using PCA.

PCA is a powerful statistical technique for analyzing complex datasets and extracting meaningful patterns. Some earlier studies use Principal Component Analysis (PCA) to explore complex relationships among multiple variables in cosmological datasets. For instance, Einasto et al. (2011) employ PCA to examine the properties of SDSS DR7 superclusters. Chaves-Montero and Hearin (2020) utilize PCA to investigate how the intricate interplay of star formation history, metallicity evolution, and dust properties influence present-day galaxy colours. Balaguera-Antolínez et al. (2024) apply PCA to analyze the sensitivity of scaling relations between various halo properties with respect to their environment. PCA offers several advantages over the traditional statistical measures for studying correlations between variables. Galaxy properties are often characterized by a large number of variables, making it challenging to interpret their relationships. By transforming the original variables into a smaller set of orthogonal components, PCA can reveal the underlying structure of relationships. PCA effectively captures the maximum variance in the data, allowing us to focus on the most significant relationships while discarding noise. Further, it can reveal emergent behaviours not immediately apparent from studying individual properties, as the components reflect combined contributions. We will carry out a comparative analysis of the principal components and their relationships with different galaxy properties across different cosmic web environments. This could provide valuable insights into the significance of the physical processes that influence galaxy evolution within distinct cosmic web environments.

The paper is structured as follows: Section 2 describes the data, Section 3 outlines the analysis method, Section 4 discusses the results, and Section 5 presents the conclusions.

In this study, we adopt a  $\Lambda$ CDM cosmology with  $\Omega_m = 0.315$ ,  $\Omega_\Lambda = 0.685$ , and  $h = 0.674$  (Planck Collaboration et al., 2020). These parameters are used to convert redshifts to comoving distances throughout the analysis.

## 2. Data

The SDSS (Stoughton et al., 2002) is one of the most ambitious and influential redshift surveys to date. It uses a dedicated 2.5-meter telescope at Apache Point Observatory in New Mexico. SDSS has measured the photometric and spectroscopic information of millions of galaxies, stars, and quasars across a significant portion of the sky. SDSS DR18 (Almeida et al., 2023) is the eighteenth data release of the SDSS. We download the data using *Structured Query Language* (SQL) from *CasJobs*<sup>1</sup>. We extract spectroscopic and photometric data pertaining to galaxies from the *SpecObj*, *PhotoObj*, and *Photoz* tables. We restrict our search to galaxies with the *scienceprimary* flag set to 1, ensuring inclusion of those with the highest-quality spectroscopic data. In our analysis, we utilize observed

---

<sup>1</sup><https://skyserver.sdss.org/casjobs/>

colours that have not been corrected for reddening caused by redshift or internal extinction. We quantify morphology of galaxies using the concentration index  $\frac{r_{90}}{r_{50}}$  (Shimasaku et al., 2001), where  $r_{90}$  and  $r_{50}$  represent the radii containing 90% and 50% of the Petrosian flux, respectively. The  $r_{90}$  and  $r_{50}$  were retrieved from the *PhotoObj* table. The stellar mass, specific star formation rate (sSFR) and metallicity of the galaxies are derived from the table *Stellar-MassFSPSGranWideDust* (Conroy et al., 2009). sSFR represents the star formation rate per unit galaxy stellar mass. The metallicity refers to the proportion of elements heavier than Helium (Asplund et al., 2009), estimated using the Flexible Stellar Population Synthesis (FSPS) technique (Conroy et al., 2009). These properties are determined by comparing observed spectroscopic and/or photometric properties of galaxies with stellar population synthesis models. SDSS spectra are obtained through a 3 arcsec aperture covering only a fraction of the entire galaxy. One can apply corrections for the finite aperture of the SDSS fibres (Brinchmann et al., 2004). However, Conroy et al. (2009) demonstrate that relying solely on broadband photometry yields more robust results. We obtain the strength of the 4000 Å break (D4000) (Bruzual A., 1983; Balogh et al., 1999) from the *galSpecIndx* table. D4000 characterizes the mean age of the stellar population in the galaxy.

We construct a volume limited galaxy sample using the SDSS DR18 data. We identify a contiguous region in the sky between the right ascension  $135^\circ \leq \alpha \leq 225^\circ$  and declination  $0^\circ \leq \delta \leq 60^\circ$ . The volume limited sample is extracted by applying extinction-corrected and  $k$ -corrected  $r$ -band absolute magnitude cut  $-23 \leq M_r \leq -21$ , which corresponds to the redshift range  $0.0434 \leq z \leq 0.1175$  (Figure 1). We consider specific ranges of galaxy properties (Table Table 1) for the present analysis, excluding any extreme outliers. Finally, we obtain 88579 galaxies in our volume limited sample.

Galaxy property	Minimum	Maximum
$(u - r) \text{ colour}$	0.5	4.5
$\log_{10} \left( \frac{M_\star}{M_\odot} \right)$	10.0	12.0
$\log_{10}(sSFR/\text{Gyr}^{-1})$	-22	-0.2
Metallicity	0.007	0.03
$\frac{r_{90}}{r_{50}}$	1.5	4.5
D4000	0.8	2.5

Table 1: This table shows the range of different galaxy properties in our final sample.

### 3. Method

#### 3.1. Classifying different morphological environments in the Cosmic Web

We use a Hessian based classification of the cosmic web (Hahn et al., 2007; Forero-Romero et al., 2009) for the present work. This method classifies the different morphological environments of the cosmic web based on the eigenvalues and eigenvectors of the deformation tensor.

The deformation tensor  $T_{ij}$  is described by the Hessian matrix of the gravitational potential field  $\Phi$  as,

$$T_{ij} = \frac{\partial^2 \Phi}{\partial x_i \partial x_j}, \quad (1)$$

where  $x_i$  and  $x_j$  are the spatial coordinates.

We compute gravitational potential  $\Phi$  by solving the Poisson equation,

$$\nabla^2 \Phi \equiv \delta \quad (2)$$

where  $\delta = \frac{\rho - \bar{\rho}}{\bar{\rho}}$  is the density contrast. We first apply the Cloud-In-Cell (CIC) scheme on a  $256^3$  grid to construct a discrete density contrast field. The overdensity field is then Fourier transformed and smoothed using an isotropic

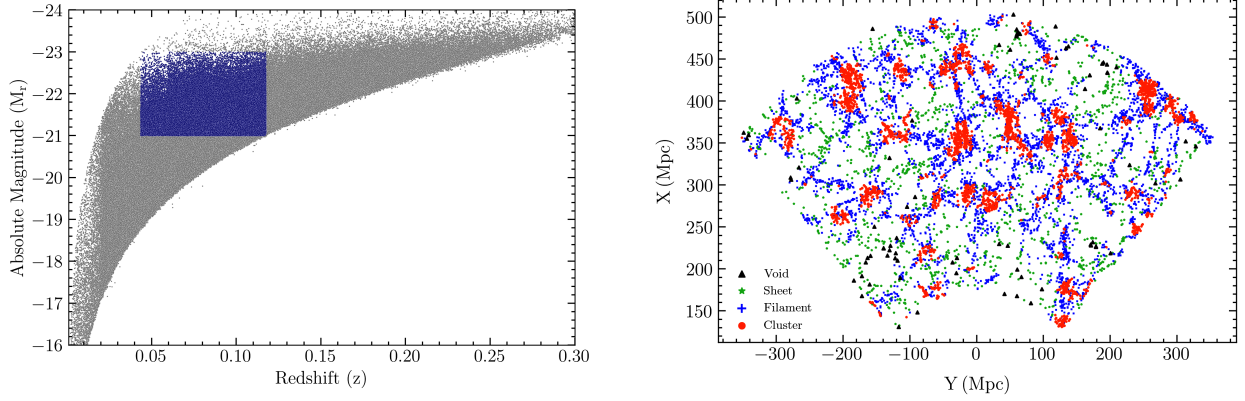


Figure 1: The left panel of this figure shows the distribution of SDSS DR18 galaxies in the redshift-absolute magnitude plane. The blue region in this diagram represents our volume-limited sample. The right panel displays a projected distribution of a 30 Mpc thick slice of this volume-limited sample in the X-Y plane. Different geometric environments of the cosmic web, identified using the Hessian-based method, are highlighted in various colours.

Gaussian filter of width 8 Mpc, which is close to the mean intergalactic separation of our galaxy sample  $\approx 8.57$  Mpc. This choice restricts our ability to characterize environments on scales smaller than the intergalactic separation. However, our approach focuses on quantifying the large-scale geometric environments within the cosmic web.

We compute the Fourier transform of the gravitational potential associated with fluctuations in the smoothed density field,

$$\hat{\Phi} = \hat{\mathcal{G}}\hat{\rho} \quad (3)$$

In this approach,  $\hat{\mathcal{G}}$  represents the Fourier transform of the Green's function of the Laplacian operator, and  $\hat{\rho}$  denotes the density in Fourier space. We transform the potential back into real space and then compute the tidal tensor using numerical differentiation. Based on the signs of its three eigenvalues ( $\lambda_1, \lambda_2, \lambda_3$ ), we categorize each galaxy into voids, sheets, filaments, or clusters. Each galaxy is classified as a part of

1. void , if  $\lambda_1, \lambda_2, \lambda_3 < 0$
2. sheet , if  $\lambda_1 > 0, \lambda_2, \lambda_3 < 0$
3. filament , if  $\lambda_1, \lambda_2 > 0, \lambda_3 < 0$
4. cluster , if  $\lambda_1, \lambda_2, \lambda_3 > 0$

where  $\lambda_1 > \lambda_2 > \lambda_3$ . The total number of galaxies in our volume limited sample, residing in voids, sheets, filaments and clusters are listed in Table 2.

Cosmic Web Environment	Number of Galaxies
Void	1273
Sheet	14597
Filament	45028
Cluster	27681

Table 2: This table provides the number of galaxies identified in different cosmic web environments.

We utilize the entire volume-limited sample consisting of 88579 galaxies to identify the various morphological components of the cosmic web.

Galaxy properties are strongly influenced by mass, necessitating careful consideration to avoid bias in any correlation studies. Differences in correlations across various geometric environments may stem from varied stellar mass

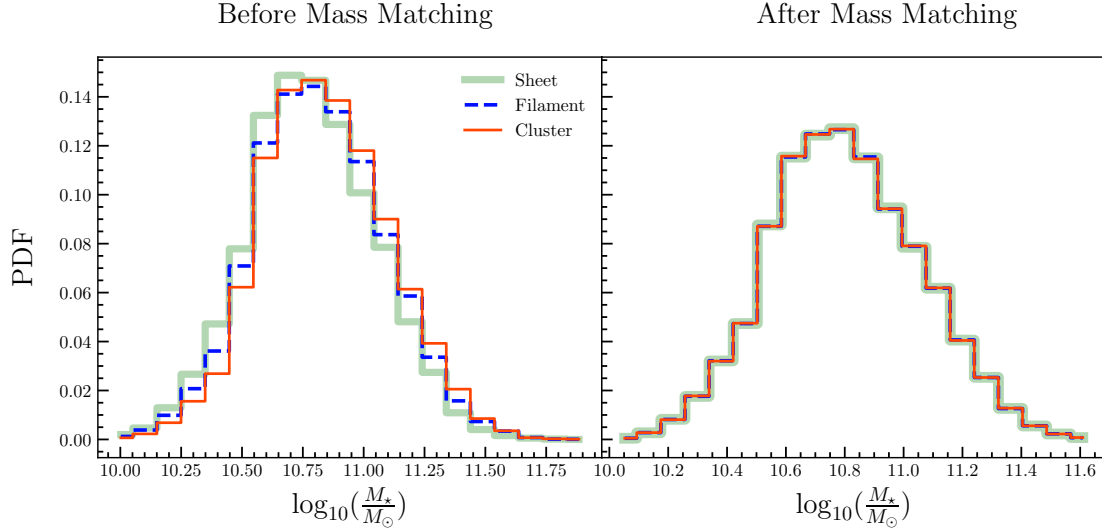


Figure 2: The left panel of this figure compares the PDFs of  $\log_{10}(\frac{M_*}{M_\odot})$  for the galaxies in different cosmic web environments. The right panel shows the same but after matching the stellar mass of galaxies in different environments.

distributions in different regions of the cosmic web. We mitigate this issue by matching the stellar mass distribution in different types of environments. We ensure that an equal number of galaxies from each of the three geometric environments are matched in terms of their stellar masses, with a precision of 0.001 dex. We show the PDF of  $\log_{10}(\frac{M_*}{M_\odot})$  for galaxies in different cosmic web environments in the left and right panels of Figure 2 before and after the mass-matching respectively. The stellar-mass matching yeields 14339 galaxies each in sheets, filaments and clusters. It may be noted that the final number of matched galaxies in other environments are not exactly equal the number of galaxies present in sheets (Table 2). This difference arises because not every galaxy in the reference sample (sheet in this case) meets our mass matching criteria. We do not consider the voids due to the very small number galaxies present within them. After the mass-matching, we perform a KS test to assess the statistical significance of the differences in the stellar mass distribution of galaxies from sheets, filaments and clusters. We observe that the null hypothesis can be confidently accepted at a significance level exceeding 99.99% for each pair of environment. The test confirms that the stellar mass distributions in our mass-matched sample are statistically indistinguishable across different environments. The mass-matched sample finally consists of 43017 galaxies from three different cosmic web environments. The analysis throughout the rest of the paper is based on this stellar mass-matched sample.

### 3.2. Principal Component Analysis (PCA)

PCA (Pearson, 1901) is a statistical technique used to reduce the dimensionality of data while retaining as much variance as possible by transforming the original variables into a new set of uncorrelated variables called principal components. Here, we briefly describe the steps involved in our analysis.

We consider a dataset  $X$  consisting of  $n$  observations (rows) and  $p$  variables (columns). In this analysis, our dataset  $X$  comprises 43017 observations of 6 variables. These observations represent all galaxies in our mass-matched volume limited sample, for which we gathered data on six distinct physical properties: colour, stellar mass, specific star formation rate (sSFR), metallicity, concentration index, and the D4000.

First, we center the data  $X$  by subtracting the mean from each column, and then divide each element by the standard deviation of the respective column as,

$$X'_{ij} = \frac{X_{ij} - \mu_j}{\sigma_j}, \quad (4)$$

where  $\mu_j = \frac{1}{n} \sum_{i=1}^n X_{ij}$  is the mean and  $\sigma_j = \sqrt{\frac{1}{n-1} \sum_{i=1}^n (X_{ij} - \mu_j)^2}$  is the standard deviation for each column. Here  $i$  corresponds to rows ( $n$  galaxies) and  $j$  corresponds to columns ( $p$  physical properties).

We then compute the covariance matrix of the standardized data as,

$$S = \frac{1}{n-1} X'^T X', \quad (5)$$

where  $X'^T$  denotes the transpose of  $X'$ . Here,  $S$  is the covariance matrix among the variables of the data matrix and it has a size of  $p \times p$ . We determine the eigenvectors and the eigenvalues of the covariance matrix  $S$ .

PCA aims to find a set of orthogonal vectors (principal components) that capture the maximum variance in the data. These principal components correspond to the eigenvectors of the covariance matrix  $S$ . Let  $v_1, v_2, \dots, v_p$  be the eigenvectors of  $S$ , and  $(\lambda_1, \lambda_2, \dots, \lambda_p)$  be the corresponding eigenvalues. The eigenvalues represent the variance explained by each eigenvector. We order the principal components by the amount of variance they explain. This simply corresponds to the magnitude of their eigenvalues. The first principal component (PC1) captures the most variation in the data and the subsequent components (PC2, PC3,...) explain the remaining variation in descending order of importance.

The eigenvectors derived from the covariance matrix can be arranged into a matrix, where each column corresponds to an eigenvector. We multiply the standardized data matrix with this eigenvector matrix. Each column of the resulting matrix represents a principal component. Thus the  $i^{th}$  principal component is given by  $PC_i = X' v_i$ , where  $X'$  is the standardized data matrix and  $v_i$  is the  $i^{th}$  eigenvector. Each principal component is a linear combination of the original variables, weighted by the elements of the corresponding eigenvector. The weight or the coefficient of any particular variable in this combination tells us the importance of that variable in defining that component. We analyze how individual galaxy properties relate to specific principal components across different cosmic web environments. This may provide valuable insights into the physical processes governing galaxy evolution in different geometric environments. This would also enable us to explore how different galaxy properties relate to each other in terms of variance captured by the principal components in different environments.

### 3.3. Normalized Mutual Information (NMI)

Mutual information (MI) is a non-parametric measure from information theory capable of identifying various forms of relationships, including those that are non-linear and non-monotonic. MI does not rely on any specific assumptions regarding the distributions. Consequently, it is generally regarded as a more general and robust measure of association compared to the Pearson or Spearman correlation coefficient (Spearman, 1904).

Consider a discrete random variable  $X$  with  $n$  possible outcomes, denoted as  $\{X_i : i = 1, \dots, n\}$ . Let  $P(X_i)$  represent the probability of the  $i^{th}$  outcome. The information entropy (Shannon, 1948) for  $X$  is defined as,

$$H(X) = - \sum_{i=1}^n P(X_i) \log P(X_i). \quad (6)$$

Here, we choose the base of the logarithm to be 10.

Now, let  $X$  and  $Y$  be two discrete random variables representing different galaxy properties. The joint entropy of  $X$  and  $Y$  is given by,

$$H(X, Y) = - \sum_{i=1}^{n_1} \sum_{j=1}^{n_2} P(X_i, Y_j) \log P(X_i, Y_j). \quad (7)$$

In our analysis, we use  $n_1 = n_2 = 20$ . The joint probabilities  $P(X_i, Y_j)$  for different values of  $X_i$  and  $Y_j$  are computed from the joint distribution of the two random variables. These joint probabilities represent the normalized abundance of galaxies within specific ranges of  $X$  and  $Y$ .

MI between  $X$  and  $Y$  is calculated as,

$$I(X; Y) = H(X) + H(Y) - H(X, Y) \quad (8)$$

MI measures how much information one variable provides about another, irrespective of the nature of their relationship. It does not assume a linear relationship between  $X$  and  $Y$ . When  $X$  and  $Y$  are statistically independent, the mutual information is zero.

The normalized mutual information (NMI) (Strehl and Ghosh, 2002) is a normalized measure of mutual information, defined as,

$$NMI(X; Y) = \frac{I(X; Y)}{\sqrt{H(X)H(Y)}} \quad (9)$$

The NMI value spans from 0 to 1, where a value of 1 signifies a strong association between the variables, and a value of 0 indicates no association.

Entropy can be sensitive to the choice of binning, but this issue is mitigated if comparisons are made using a consistent number of bins. In our analysis, we maintain the same number of bins and the same number of galaxies for each type of geometric environment. This approach ensures that shot noise contributes equally across different environments, allowing for meaningful comparisons of results.

In this study, we will analyze the NMI between the principal components and galaxy properties across various geometric environments. Our goal is to determine whether these relationships differ in a statistically significant way.

## 4. Results

### 4.1. Analyzing the correlations between different galaxy properties with Spearman's rank correlation

Different galaxy properties are interrelated with each other. We first study the correlations between various galaxy properties in our combined sample using Spearman's rank correlation coefficient. The Spearman's rank correlation coefficient is a nonparametric measure that can quantify the statistical dependence between the rankings of two variables, gauging the extent to which their relationship can be characterized by a monotonic function. In other words, it evaluates whether the variables tend to change together in the same direction without assuming they change in a linear fashion. Spearman's rank correlation is thus suitable for assessing relationships that are monotonic but not necessarily linear. This allows for a more comprehensive data analysis, capturing nonlinear associations that may exist between different galaxy properties. The Spearman's rank correlation coefficient ranges from  $-1$  to  $1$ . If the value of the correlation coefficient is  $1$ , it indicates a perfect positive correlation between two variables, implying that as one variable increases, the other variable increases proportionally. Conversely, a value of  $-1$  signifies a perfect negative correlation and a coefficient of  $0$  suggests no correlation between the variables.

We use Spearman's rank correlation to quantify the strength and direction of the relationships. This analysis tells us about the existing relationships between different galaxy properties in our sample. We consider the entire volume limited galaxy sample without partitioning it into distinct geometric environments. The values of Spearman's rank correlation coefficient as obtained in our analysis, are shown in Figure 3. We observe the highest positive correlation ( $\sim 0.7648$ ) between  $(u - r)$  colour and  $D4000$  and the highest negative correlation ( $\sim -0.8575$ ) between  $D4000$  and  $\log(sSFR)$ . The correlation values between metallicity and other properties are notably low. This is also corroborated by the scatter plots in Figure 3. We can observe considerable dispersion between metallicity and other galaxy properties.

This analysis provides us with a summary of the strength and direction of the relationships between different galaxy properties in our sample. It is clear that various galaxy properties exhibit both linear and non-linear relationships. Identifying and understanding the nature of both linear and non-linear relationships among multiple variables can be quite complex. Our primary goal in this study is to verify if the interrelationships between different galaxy properties are affected by their large-scale cosmic web environment. PCA is a powerful exploratory tool that can provide valuable insights into the structure of data and relationships between multiple variables exhibiting complex patterns. In the next subsection, we utilize PCA to investigate the structure and relationships among galaxy properties in our volume-limited sample. Additionally, we compare both the principal components and their individual relationships with different galaxy properties across various geometric environments within the cosmic web.

### 4.2. Understanding structure and relationships in the data using Principal Component Analysis

Our data matrix consists of  $(u - r)$  colour,  $\log_{10}(\frac{M_{\star}}{M_{\odot}})$ ,  $\log_{10}(sSFR)$ , metallicity,  $\frac{r_{90}}{r_{50}}$ ,  $D4000$  for 43017 galaxies in our volume limited sample. We first standardize the data matrix following the method described in subsection 3.2. Subsequently, we calculate the covariance matrix and determine its eigenvalues and eigenvectors. The elements of the eigenvectors and the associated galaxy properties are described in Table 3. PCA converts the set of galaxy properties to a new set of uncorrelated components, known as the principal components (subsection 3.2). Each



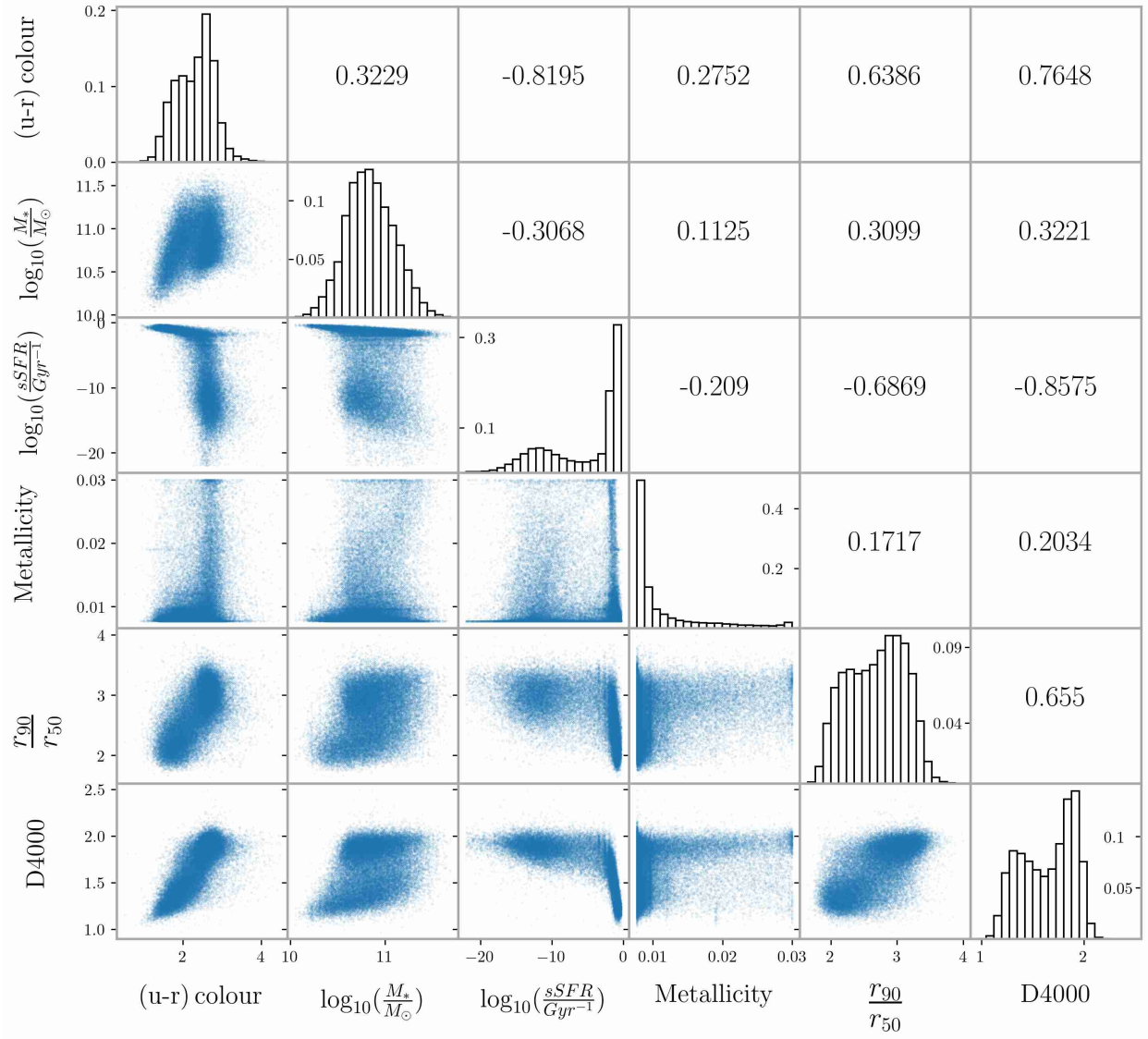


Figure 3: The lower diagonal panels of this plot show the scatter plots for the different pairs of galaxy properties. The panels in the upper diagonal show the Spearman's rank correlation coefficients for the respective pairs of galaxy properties. The diagonal panels show the PDF for individual galaxy properties.

principal component is a linear combination of the six galaxy properties. The coefficients of the linear transformation determine the contribution of each property to a particular principal component. The largest variance of the data set lies along the first principal component, while subsequent components capture decreasing amounts of variance.

After performing PCA, we obtain a set of eigenvalues, each corresponding to a principal component and representing the amount of variance explained by that component. The percentage of explained variance is calculated by dividing each eigenvalue by the sum of all the eigenvalues and then multiplying by 100. This straightforward calculation allows us to quantify how much variance each component accounts for in the overall dataset. We show the percentage of variance captured by the different principal components in Table 4. Approximately 85% of the variance in our data matrix is explained by the first three principal components. With this in mind, our focus shifts to examining the behaviors of PC1, PC2, and PC3 across different cosmic web environments. Additionally, we investigate how principal components PC1, PC2 and PC3 relate to various galaxy properties within these diverse geometric environments. We describe the results of these analysis in the following subsection.

Properties	$v_1$	$v_2$	$v_3$	$v_4$	$v_5$	$v_6$
$(u - r)$ colour	0.4836	-0.0686	-0.0192	0.2725	0.7580	0.3351
$\log_{10}(\frac{M_*}{M_\odot})$	0.2681	0.5357	0.7697	0.1029	-0.1769	0.0831
$\log_{10}(\frac{sSFR}{\text{Gyr}^{-1}})$	-0.4508	0.3698	0.1248	-0.2731	0.6156	-0.4369
Metallicity	0.2172	0.7364	-0.6258	0.0701	-0.1177	0.0107
$\frac{r_{90}}{r_{50}}$	0.4464	-0.0516	-0.0056	-0.8914	0.0050	0.0585
$D4000$	0.4945	-0.1631	-0.0049	0.2026	-0.0370	-0.8285

Table 3: The weights or coefficients of each original variable in the linear combinations that form the principal components are the elements of the corresponding eigenvector. This table shows the elements of the eigenvector obtained from the combined stellar mass-matched sample.

Principal Component	Percentage of Variance Explained
PC1	55.21
PC2	16.25
PC3	13.14
PC4	7.06
PC5	4.79
PC6	3.55

Table 4: This table represents the percentage of variance explained by individual principal component.

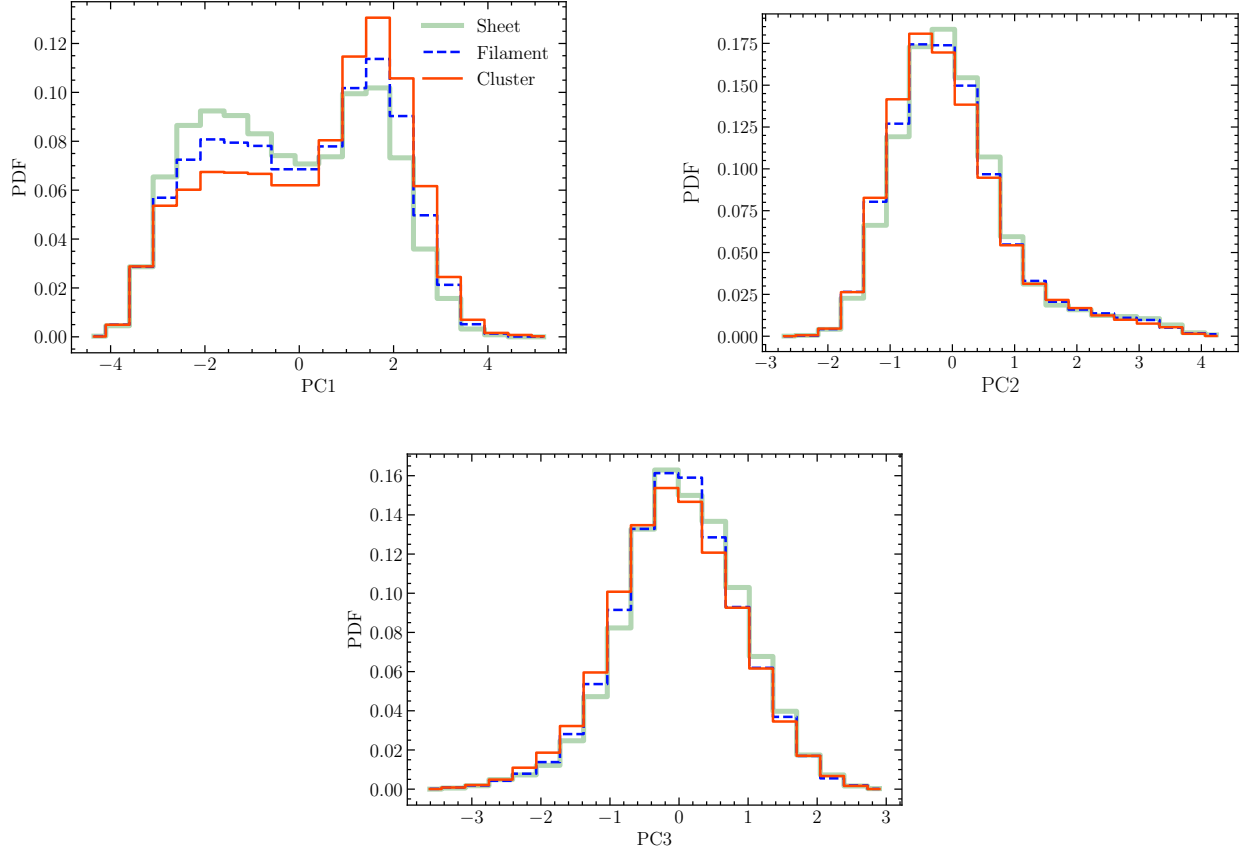


Figure 4: The top left, top right and bottom panels of this figure respectively compares the PDFs of PC1, PC2 and PC3 in different geometric environments.

Web Environments	$p$ -value
Sheet-Filament	$8.22 \times 10^{-24}$
Filament-Cluster	$5.67 \times 10^{-29}$
Sheet-Cluster	$2.75 \times 10^{-98}$

Table 5: KS test results for PC1

Web Environments	$p$ -value
Sheet-Filament	$9.42 \times 10^{-6}$
Filament-Cluster	$4.85 \times 10^{-5}$
Sheet-Cluster	$2.63 \times 10^{-17}$

Table 6: KS test results for PC2

Web Environments	$p$ -value
Sheet-Filament	$7.45 \times 10^{-6}$
Filament-Cluster	$9.71 \times 10^{-8}$
Sheet-Cluster	$2.30 \times 10^{-18}$

Table 7: KS test results for PC3

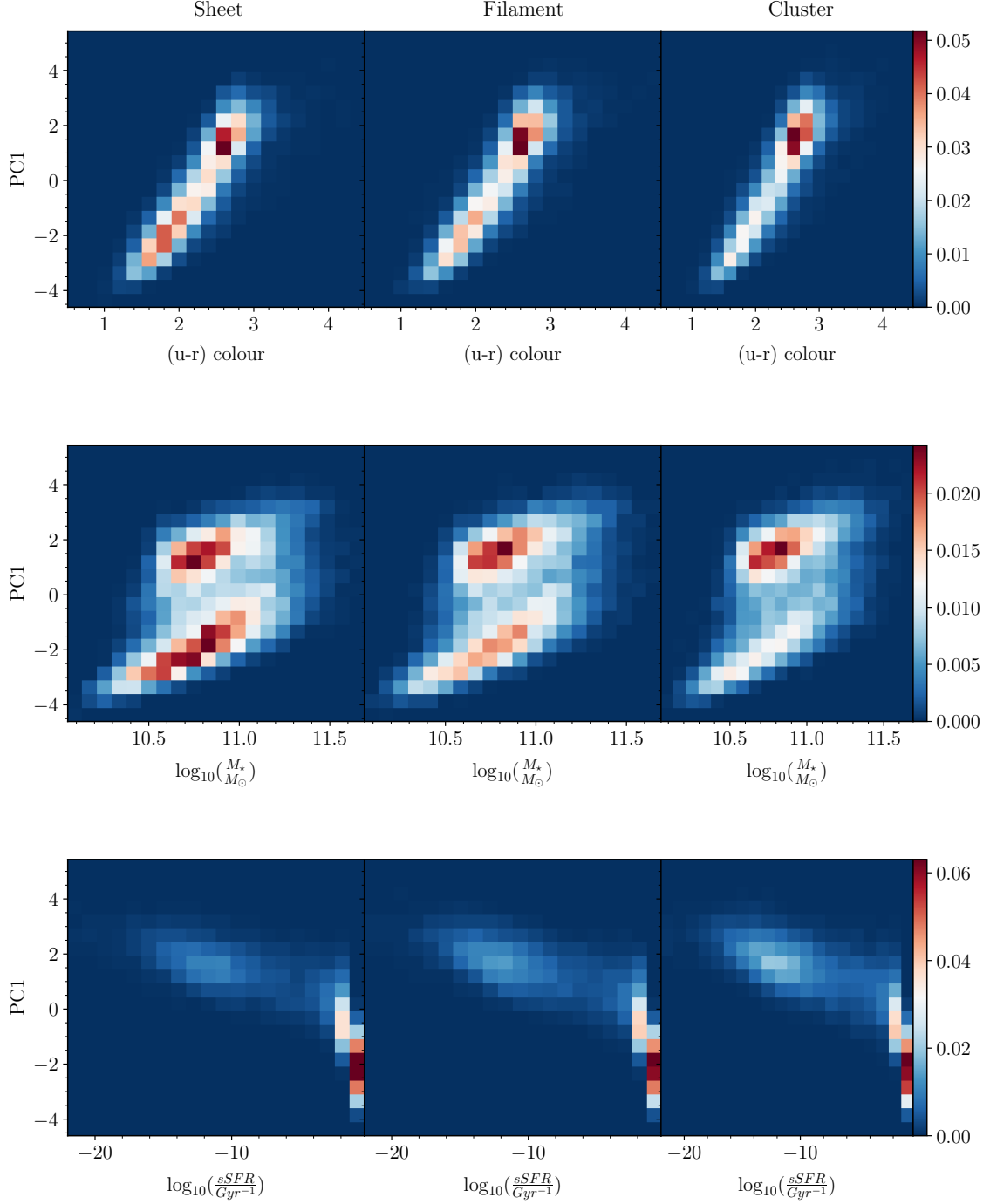


Figure 5: The top panels of this figure show the joint PDFs of PC1 and  $(u-r)$  colour across three cosmic web environments. The middle and lower panels show the same but for  $\log_{10}(\frac{M_*}{M_{\odot}})$  and  $\log_{10}(\frac{sSFR}{\text{Gyr}^{-1}})$  respectively.

#### 4.3. Comparing the principal components in different cosmic web environments

We categorize galaxies into various cosmic web environments and compute PC1, PC2, and PC3 using eigenvectors derived from the entire dataset for each environment. In the top left panel of Figure 4, we compare the PDFs of PC1 across filaments, sheets, and clusters. PC1 displays clear bimodality in all cosmic web environments, with two distinct peaks symmetrically positioned around  $PC = 0$ . The amplitudes of these peaks differ across environments: sheets exhibit the highest amplitude for the peak at negative PC1, followed by filaments and clusters. The trend reverses for the peak at positive PC1. The observed bimodality in the PDF of PC1 reflects underlying structure where two distinct groups of galaxies are present. This finding is consistent with the observed bimodality in many galaxy properties like colour, sSFR, morphology and star formation history. Interestingly, these four galaxy properties have the dominant contribution to PC1 as compared to the other two properties (stellar mass and metallicity). The symmetrical location of the two peaks around  $PC1 = 0$  suggests that the two groups of galaxies are roughly equal in size and have contrasting physical characteristics.

PC1 encapsulates the interplay between sSFR, colour, morphology, and D4000 in shaping galaxy bimodality, emphasizing how star formation and aging processes co-evolve differently in different cosmic web environments. The bimodality in PC1 reflects how environmental processes act collectively to separate galaxies into star forming and quenched groups.

In the top right panel of Figure 4, we compare the PDFs of PC2 across different environments. PC2 is dominated by metallicity and exhibit a unimodal distribution across all environments, indicating less variability compared to PC1. Interestingly, the PDFs of PC2 in each environment is asymmetrical around  $PC2 = 0$  and has an extended tail towards the positive PC2 values. This aligns with the mass-metallicity relation, where lower-mass, more numerous galaxies tend to have lower metallicities, while high-metallicity galaxies are rarer and more massive. The positive skewness in PC2 possibly also captures subtler environmental influences on secondary processes like chemical enrichment.

We compare the PDFs of PC3 across different environments in the bottom panel of Figure 4. The distributions are unimodal in each environment. However, they exhibit an extended tail towards the negative PC3 values. PC3 is dominated by stellar mass. The negatively skewed distribution indicates a concentration of high-mass galaxies and a tail toward low masses. It also suggests that lower-mass galaxies contribute less distinctive variation once PC1 and PC2 are accounted for.

Thus PC1 highlights clear differences among galaxy properties in different cosmic web environments whereas PC2, PC3 capture a more continuous variation in physical properties with a positive skewness. We assess the statistical significance of the differences in PDFs of PC1, PC2 and PC3 across various cosmic web environment. The results of the KS tests are detailed in Table 5, Table 6, and Table 7 respectively. The tables show that the null hypothesis can be rejected at  $> 99.99\%$  confidence level in all cases suggesting that the first three principal components are distinctly different in various geometric environments of the cosmic web. The fact that PC1, PC2, PC3 behave differently across cosmic web environments implies that the spatial arrangement of galaxies in sheets, filaments, or clusters have a measurable impact on their physical properties.

#### 4.4. Comparing the correlations between principal components and galaxy properties in different geometric environments

Principal components are linear combinations of various galaxy properties, so their relationships might be approximately linear. However, no galaxy property is perfectly correlated with the principal components. The complex interplay between different galaxy properties and their varying contributions to the principal components indicates that modeling principal components as a linear function of any single galaxy property would capture only part of the overall picture. Generally, the relationship can be non-linear if other galaxy properties significantly influence the principal components. With this in mind, we use normalized mutual information (NMI) to explore the individual relationships between each principal component and galaxy property.

We show the joint probability distributions of PC1 with the six different galaxy properties across various geometric environments in Figure 5 and Figure 6. In each environment, the various panels of these figures indicate that the  $(u-r)$  colour,  $\frac{r_{90}}{r_{50}}$ , and D4000 show positive correlations with PC1. Conversely,  $\log_{10}(\frac{sSFR}{Gyr^{-1}})$  exhibits a negative correlation with PC1 in all environments. It may be noted here that NMI does not provide any direction of the correlations unlike Pearson correlation coefficient. However, one can find the general trends by inspecting the sign of the corresponding element of the eigen vector (representing PC1) or analyzing the joint PDF of PC1 and a galaxy property. The stellar

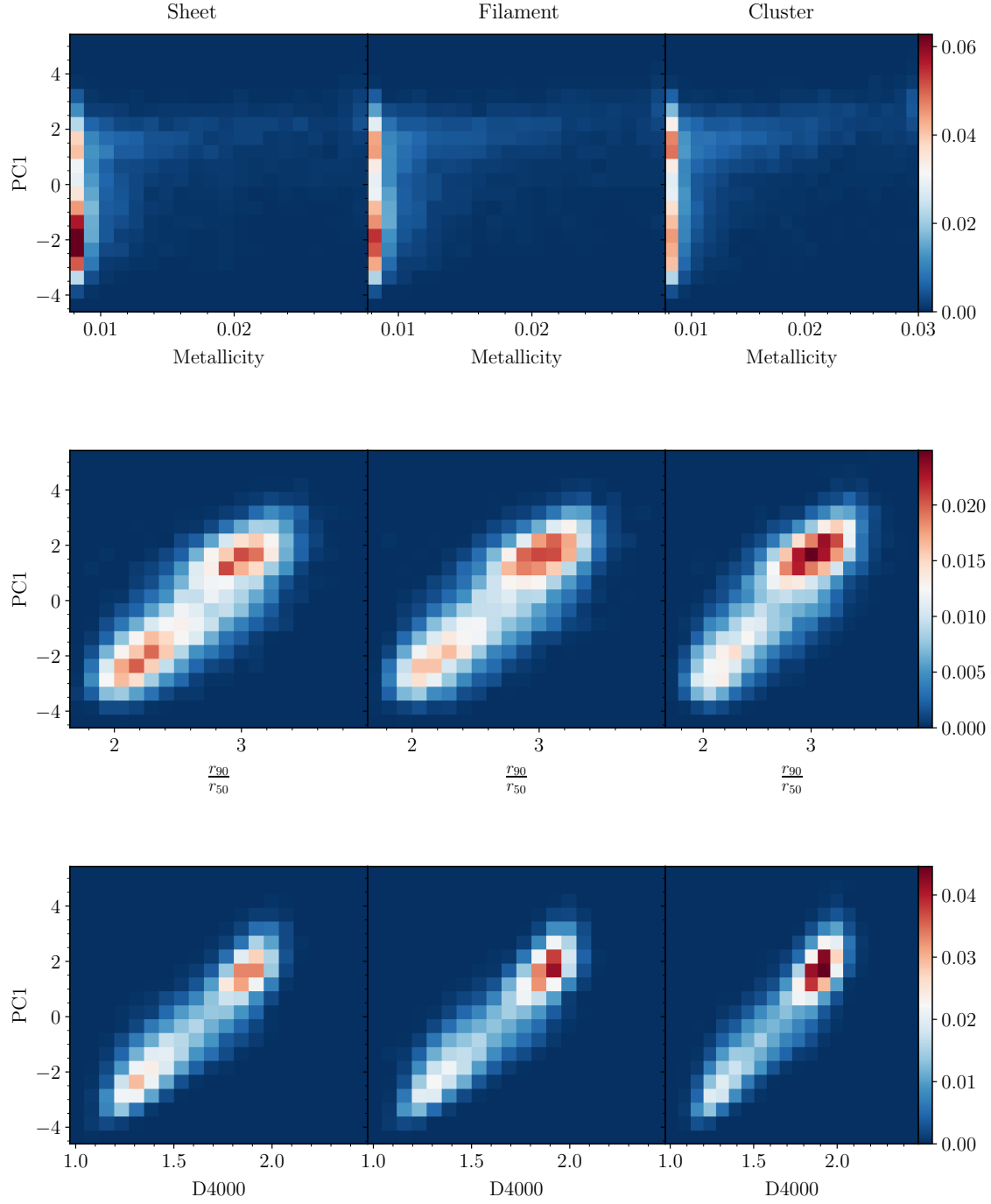


Figure 6: Same as Figure 5 but for metallicity, concentration index and D4000.

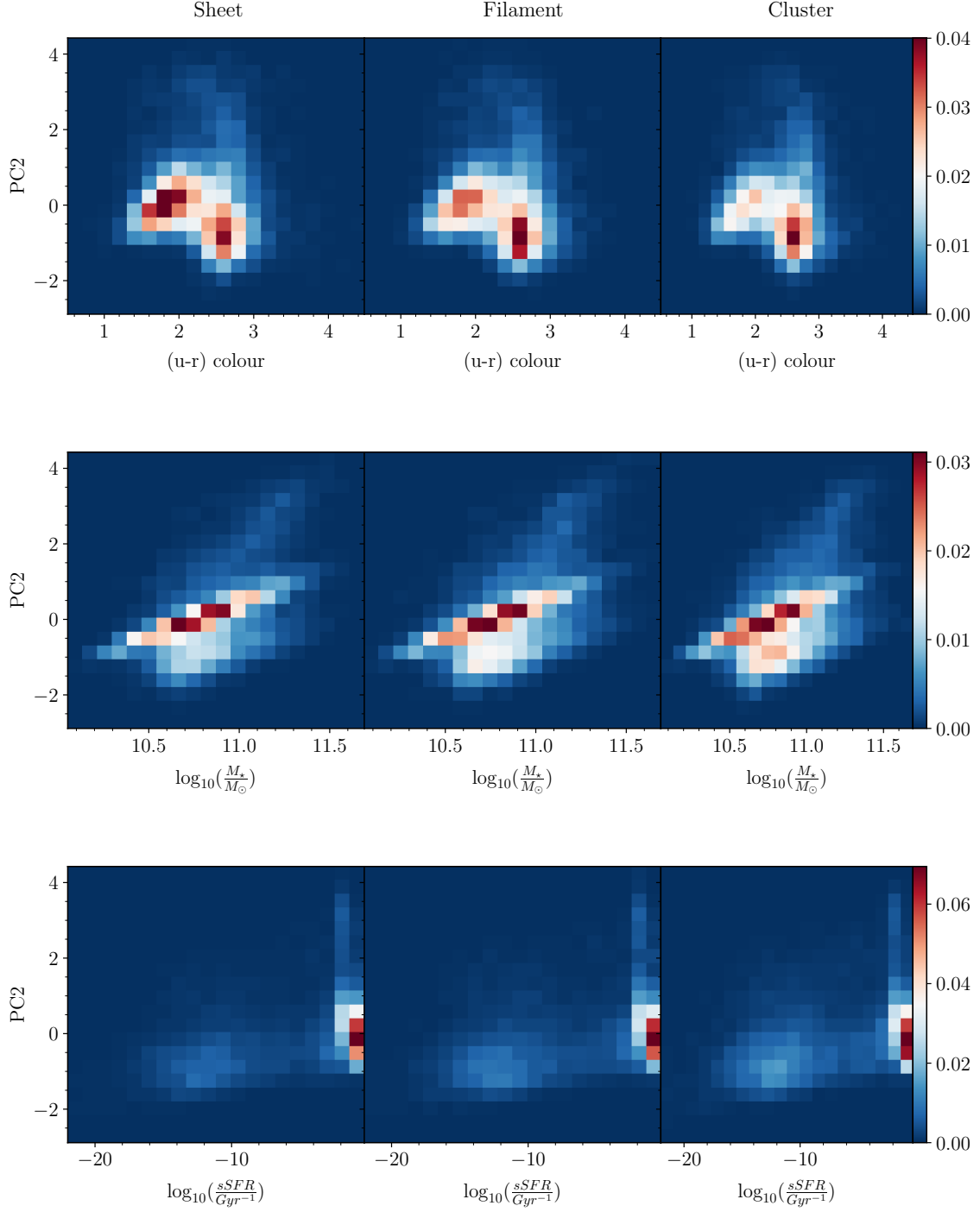


Figure 7: Same as Figure 5 but for PC2.

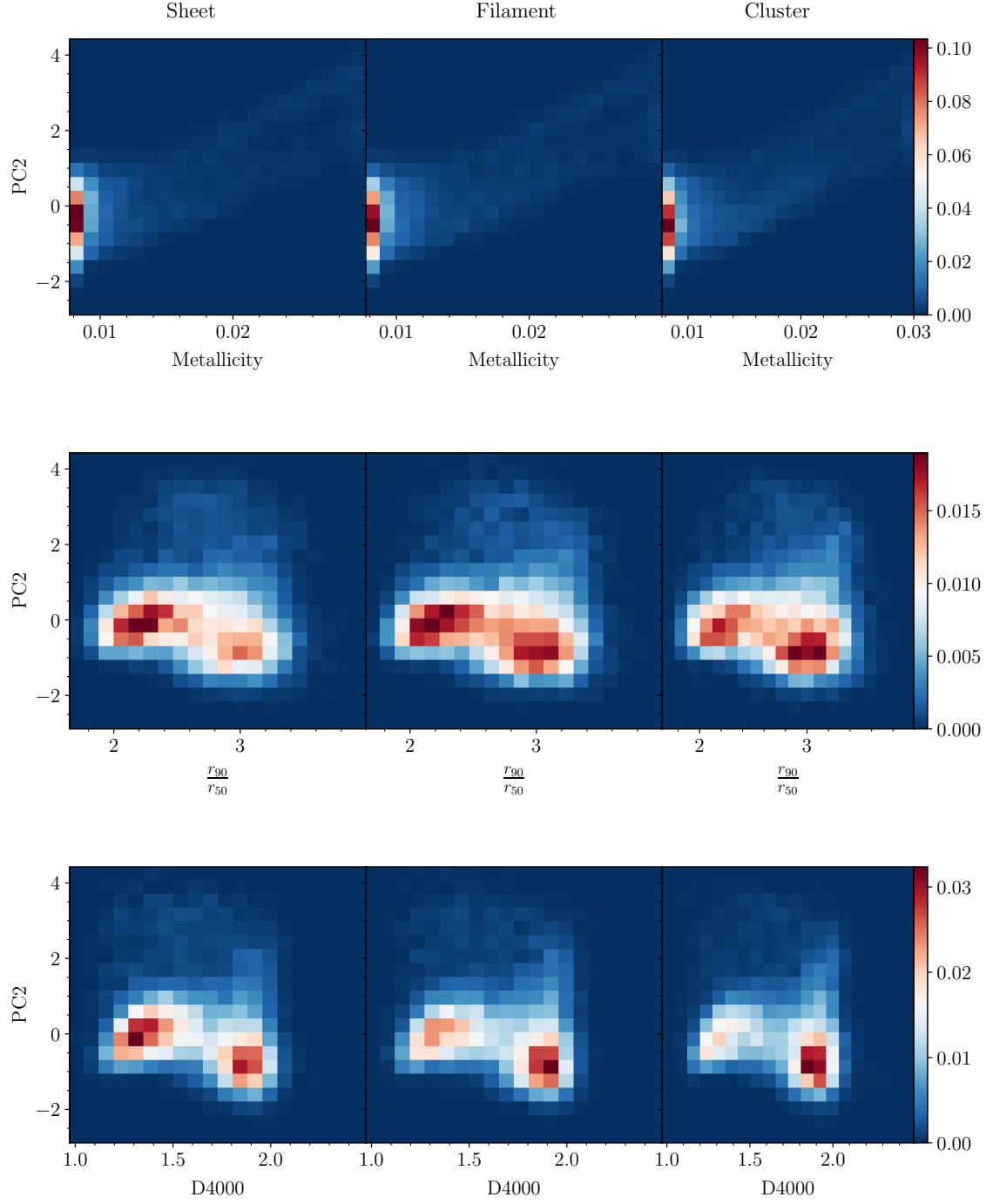


Figure 8: Same as Figure 6 but for PC2.



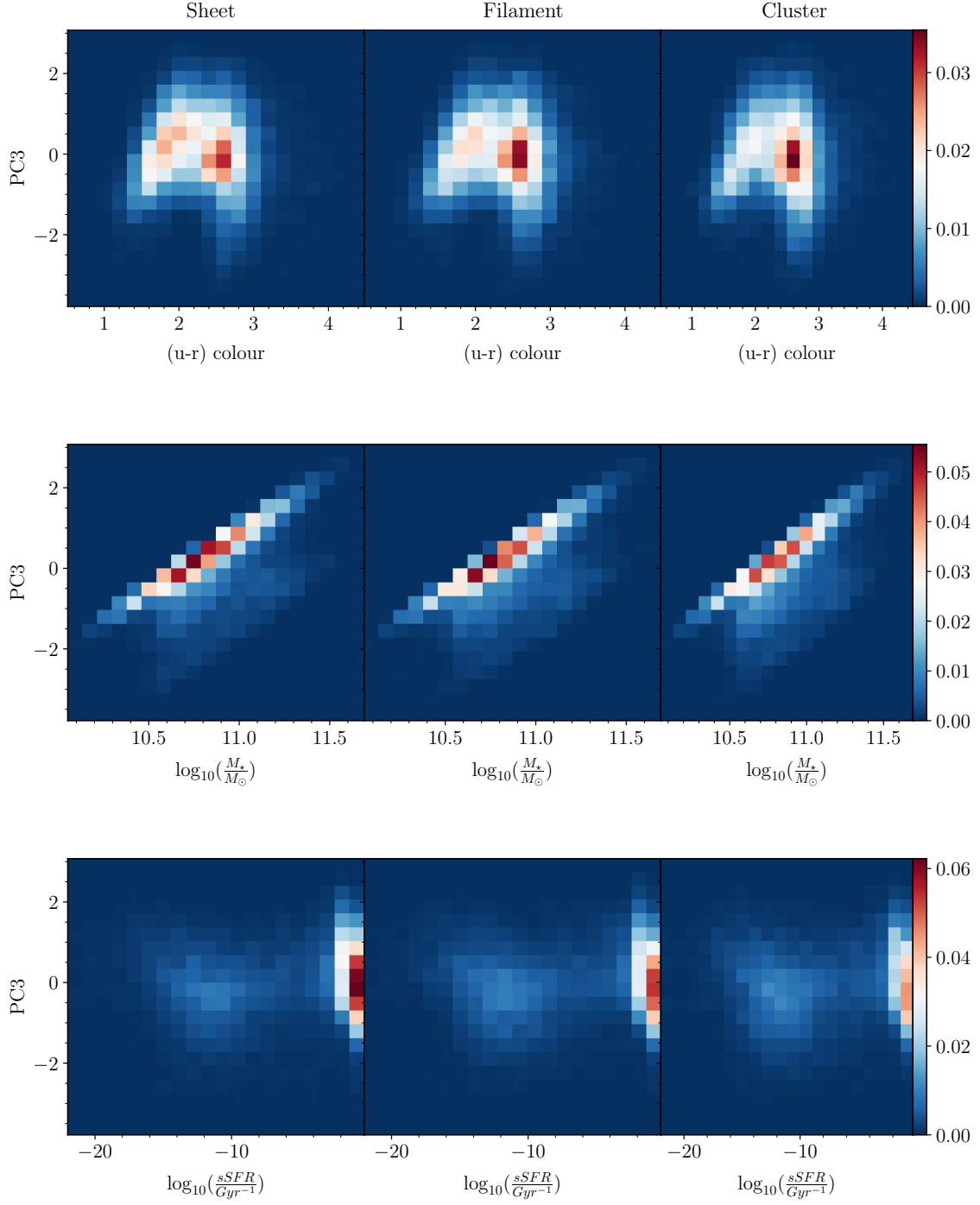


Figure 9: Same as Figure 5 but for PC3.

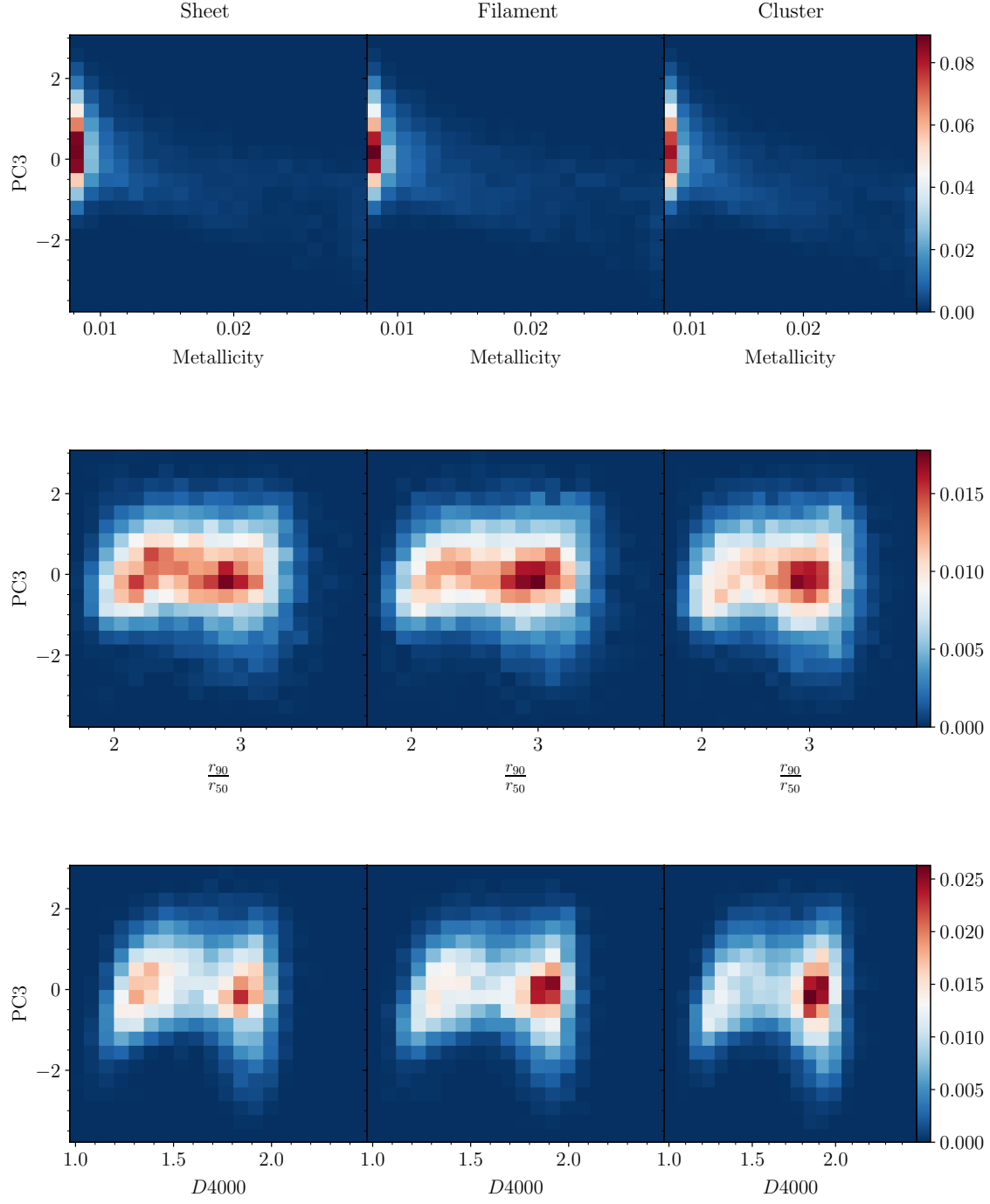


Figure 10: Same as Figure 6 but for PC3.

mass and metallicity exhibit a positive correlation with PC1. However their relationships seems to be more complex. These trends are consistent with the sign and magnitude of the elements of the first eigenvector  $v_1$  shown in Table 3. The various panels in Figure 5 and Figure 6 demonstrate that the joint PDFs of PC1 and different galaxy properties are sensitive to the geometric environments. It may be noted that we use the exact same number of mass-matched galaxies from each cosmic web environment.

It is well established that galaxies rich in gas typically exhibit higher star formation rates, bluer colours, younger stellar populations, and disk-like morphologies. Our analysis reveals that the correlations between PC1 and properties related to star formation, gas content, or morphology vary significantly across different cosmic web environments. This variability reflects how galaxy properties are influenced by factors such as gas accessibility, galaxy interactions, the effectiveness of various quenching mechanisms, and tidal interactions. Untangling the individual contributions of each of these factors to the observed differences in the joint distributions is extremely challenging. We present the joint PDFs for PC2 and different galaxy properties in Figure 7 and Figure 8. Similarly, the joint PDFs of PC3 and different galaxy properties are shown in Figure 9 and Figure 10. These figures reveal that the shapes and spreads of the joint PDFs are markedly influenced by the cosmic web environments. These variations underscore the significant impact of geometric environments on shaping galaxy properties and their interrelationships.

We measure the NMI between the principal components (PC1, PC2 and PC3) and the individual galaxy properties, and then assess the statistical significance of the differences in its value across different cosmic web environments. To do this, we generate 50 jackknife samples from the original data by randomly sampling 80% of the galaxies each time, without replacement. We estimate the principal components from each of these 50 jackknife samples and calculate the normalized mutual information (NMI) (subsection 3.3) between the principal components and the individual galaxy properties. We then use a two-tailed t-test to determine if there is a significant difference between the mean NMI values across different pairs of geometric environments. The results of our test for PC1, PC2 and PC3 are presented in Table 8, Table 9, and Table 10 respectively. We observe that the p-value for each relationship in every pair of geometric environments is extremely small ( $< 10^{-4}$  in nearly all cases), indicating that the measured NMI for any relationship is significantly different ( $> 99.99\%$  confidence level) across various cosmic web environments. The very small p-values observed in our analysis are likely a consequence of the large sample size and the increased statistical power it provides. These small values indicate that the correlations detected between principal components and galaxy properties across different cosmic web environments are statistically robust and unlikely to have arisen by chance. However, while the statistical significance is evident, the physical significance requires careful interpretation. In the context of galaxy evolution in the cosmic web, even weak correlations can be physically meaningful if they point to consistent environmental trends. These subtle trends can reveal important clues about mechanisms like gas accretion, quenching, or galaxy interactions, which operate differently depending on the large-scale cosmic web environment. Therefore, identifying and interpreting even modest correlations can be crucial for understanding how the cosmic web influences the formation and evolution of galaxies. Our analysis suggests that the cosmic web environment has a significant influence on galaxy evolution. PCA shows that galaxies in different cosmic web environments differ in complex ways that are not evident from the correlations between individual galaxy properties.

We perform these analyses using 20 bins for each variable. Additionally, we repeat the analysis with 10 and 30 bins and find that our main conclusions remain unchanged. We also repeat the entire analysis using the dataset without specifying any ranges for the galaxy properties and find that our conclusions remain the same.

## 5. Discussions and Conclusions

In this work, we use Principal Component Analysis (PCA) to investigate the influence of cosmic web environments (sheets, filaments, and clusters) on galaxy properties, focusing on the distributions of the principal components (PC1, PC2, and PC3), and their correlations with physical properties such as colour, sSFR, D4000, metallicity, and morphology. The results highlight the interplay between external environmental effects and internal secular processes in shaping galaxy evolution.

We analyze the principal components in different cosmic web environments and test if their probability distributions are different in a statistically significant manner. We also study the relationships between the different principal components and individual galaxy properties using the normalized mutual information (NMI). Our key findings are summarized as follows.

Relations	Sheet-Filament	Filament-Cluster	Sheet-Cluster
	$p$ value	$p$ value	$p$ value
PC1 - colour	$9.09 \times 10^{-60}$	$2.11 \times 10^{-28}$	$3.90 \times 10^{-73}$
PC1 - stellar mass	$9.45 \times 10^{-9}$	$2.55 \times 10^{-17}$	$2.79 \times 10^{-4}$
PC1 - sSFR	$3.97 \times 10^{-59}$	$2.26 \times 10^{-67}$	$3.93 \times 10^{-88}$
PC1 - metallicity	$4.69 \times 10^{-9}$	$5.44 \times 10^{-90}$	$6.00 \times 10^{-89}$
PC1 - concentration index	$2.14 \times 10^{-7}$	$5.61 \times 10^{-38}$	$5.79 \times 10^{-46}$
PC1 - $D4000$	$5.80 \times 10^{-52}$	$5.26 \times 10^{-50}$	$5.90 \times 10^{-79}$

Table 8: This table summarizes the results of a two-tailed t-test after comparing the normalized mutual information for the NMI between PC1 and different galaxy properties in two different cosmic web environments. The degrees of freedom in this test is  $(n_1 + n_2 - 2) = 98$ .

Relations	Sheet-Filament	Filament-Cluster	Sheet-Cluster
	$p$ value	$p$ value	$p$ value
PC2 - colour	$2.64 \times 10^{-55}$	$6.19 \times 10^{-39}$	$4.97 \times 10^{-75}$
PC2 - stellar mass	$3.16 \times 10^{-69}$	$3.32 \times 10^{-65}$	$4.12 \times 10^{-96}$
PC2 - sSFR	$2.81 \times 10^{-34}$	$3.99 \times 10^{-64}$	$1.83 \times 10^{-77}$
PC2 - metallicity	$8.05 \times 10^{-41}$	$4.01 \times 10^{-16}$	$4.05 \times 10^{-57}$
PC2 - concentration index	$5.45 \times 10^{-18}$	$7.35 \times 10^{-43}$	$3.26 \times 10^{-53}$
PC2 - $D4000$	$2.77 \times 10^{-20}$	$2.81 \times 10^{-30}$	$2.09 \times 10^{-51}$

Table 9: Same as Table 8, but for the NMI between PC2 and different galaxy properties.

Relations	Sheet-Filament	Filament-Cluster	Sheet-Cluster
	$p$ value	$p$ value	$p$ value
PC3 - colour	$5.71 \times 10^{-63}$	$3.10 \times 10^{-6}$	$2.65 \times 10^{-60}$
PC3 - stellar mass	$1.35 \times 10^{-74}$	$3.19 \times 10^{-40}$	$2.29 \times 10^{-87}$
PC3 - sSFR	$1.27 \times 10^{-14}$	$4.71 \times 10^{-19}$	$2.72 \times 10^{-35}$
PC3 - metallicity	$1.38 \times 10^{-3}$	$1.32 \times 10^{-66}$	$1.62 \times 10^{-60}$
PC3 - concentration index	0.14	$9.35 \times 10^{-5}$	0.01
PC3 - D4000	$6.57 \times 10^{-55}$	$1.52 \times 10^{-37}$	$1.60 \times 10^{-21}$

Table 10: Same as Table 8, but for the NMI between PC3 and different galaxy properties.

PC1, PC2, and PC3 respectively explains  $\sim 55\%$ ,  $\sim 16\%$ , and  $\sim 13\%$  variance in our data. PC1 shows clear bimodality in all cosmic web environments. The presence of bimodality in PC1 indicates its ability to account for most of the variance in the data. Two peaks in PC1 are symmetrically located around  $PC1 = 0$ . The nearly symmetric placement of the two peaks in all environments suggests that two groups of galaxies with contrasting physical properties are present in each cosmic web environment. It implies that bimodality in different galaxy properties can emerge in each type of geometric environment. We note that the negative PC1 peak is highest in sheets, followed by filaments, and lowest in clusters. The positive PC1 peak shows the opposite trend, highest in clusters, followed by filaments, and lowest in sheets. Thus the cosmic web environments strongly influence the distribution of PC1, with sheets favouring negative PC1 and clusters favouring positive PC1. PC1 is strongly correlated with properties directly tied to star formation activity, including colour, sSFR, D4000, and morphology. Its bimodal distribution reflects the two dominant galaxy populations: star-forming galaxies (negative PC1 values) and quenched galaxies (positive PC1 values). Dividing galaxies into two groups based on whether their PC1 values are negative or positive could be an effective method for distinguishing quenched galaxies from star-forming ones. This classification is particularly advantageous because PC1 is a linear combination of several galaxy properties, and it accounts for the bimodality observed in each of these properties, making it a more robust approach.

We note that the bimodality in PC1 is strongly sensitive to the cosmic web environment. In sheets, galaxies are predominantly star-forming, maintaining blue colours, high sSFR, disk-like morphology and younger stellar populations due to mild gravitational interactions and access to fresh gas. In clusters, by contrast, galaxies are more likely to be quenched, with redder colours, low sSFR, bulge-dominated morphology, and older stellar populations. This reflects the effectiveness of environmental mechanisms such as ram-pressure stripping, mergers, and tidal interactions in suppressing star formation.

On the other hand, PC2 and PC3 do not exhibit bimodality in any cosmic web environment. They exhibit less variability compared to PC1 across cosmic web environments, implying they are less influenced by spatial clustering. PC2 is dominated by metallicity and secondary variations in stellar mass and morphology. Unlike PC1, PC2 exhibits a unimodal and positively skewed distribution across all environments, suggesting that metallicity evolves more gradually and is less sensitive to sudden environmental changes. The weaker environmental dependence of PC2 highlights the role of internal processes, such as gradual chemical enrichment and mass growth through accretion, that proceed independently of external conditions. On the other hand, PC3 exhibit a unimodal distribution with negative skewness. It is dominated by stellar mass, implying most of the variance explained by this component comes from differences in stellar mass between galaxies after accounting for the effects captured in PC1 and PC2. It may also arise due to the fact that our volume limited sample have galaxies above a certain mass. So the low-mass galaxies will be underrepresented, skewing the distribution.

Using a KS test, we find that the null hypothesis can be rejected at  $> 99.99\%$  confidence level for PC1, PC2, PC3. This suggests that cosmic web plays a crucial role in shaping the correlations between galaxy properties. The contrasting behavior of PC1, PC2, and PC3 encapsulates the balance between external and internal processes shaping

galaxies. PC1 is highly sensitive to environment and reflects the immediate impact of the cosmic web on star formation and quenching. PC2 and PC3, by comparison, are less environment-dependent and captures longer-term, gradual processes like chemical enrichment and stellar mass growth. The use of PCA thus provides a powerful framework for understanding galaxy evolution, allowing us to capture both dominant environmental effects and subtler secular trends.

We measure the normalized mutual information between principal components and individual galaxy properties in different geometric environments of the cosmic web. We use a two-tailed t-test to compare the normalized mutual information in each pair of geometric environment. We find that for each relationship and each pair of geometric environment, the null hypothesis can be rejected at  $> 99.99\%$  confidence level.

Understanding these differences is crucial as they provide insights into how galaxies evolve and interact within their larger-scale geometric environments. It also helps refine models of galaxy formation and evolution. The cosmic web serves as a grand scaffolding that intricately organizes and molds the distribution of matter and galaxies across the vast expanse of the universe. Our analysis suggests that various morphological components of the cosmic web like filaments, sheets, clusters and voids have a significant impact on the galaxy properties and their interrelationships. The galaxies in clusters might evolve differently compared to those in filaments or sheets, affecting their observed properties and correlations. For instance, filaments are the largest known coherent structures (Pandey et al., 2011; Sarkar et al., 2023) in the cosmic web, containing a significant amount of baryonic matter, including WHIM (Nicastrò et al., 2018). Filaments host more than 80% of the WHIM in the universe (Tuominen et al., 2021; Galárraga-Espinosa et al., 2021). The continuous supply of gas can influence the star formation rates, chemical enrichment, and overall evolution of galaxies residing within filaments. Further, studies with high-resolution zoom-in hydrodynamical simulations by Liao and Gao (2019) show that gas accretion onto filament halos is highly anisotropic, leading to higher baryon and stellar fractions compared to galaxies in the field. The low-mass halos typically accrete matter perpendicular to their host filament, while high-mass halos mainly accrete along the axis of the filament (Ganeshaiah Veena et al., 2018). Numerous studies based on observational and simulations (Kuutma et al., 2017; Malavasi et al., 2017; Laigle et al., 2018; Kraljic et al., 2018; Bonjean et al., 2020) have consistently shown that galaxies near filament spines are redder, more massive, and less star-forming than their counterparts, even at fixed environmental density. This trend is commonly attributed to enhanced gas accretion, more frequent galaxy-galaxy interactions, and increased merger rates in these regions, which collectively drive rapid stellar mass growth. Cosmological and hydrodynamical simulations (Singh et al., 2020; Song et al., 2021; Malavasi et al., 2022; Kotecha et al., 2022) lend strong support to this interpretation. These differences could be reflected in the PCA results as distinct patterns or correlations between the principal components and galaxy properties. The strong correlations of PC1 with colour, sSFR, morphology, and D4000 can be interpreted as evidence that environmental processes drive star formation and aging. The bimodality in PC1 provides direct evidence of environmental effects, with negative PC1 values reflecting sustained star formation in sheets and filaments, and positive PC1 values reflecting quenching in clusters. The positive skewness of PC2, the negative skewness of PC3 and their weaker environmental dependence suggest that properties like metallicity and stellar mass evolve more gradually across different cosmic web environment.

It is important to acknowledge some caveats in our analysis. We conduct our study in redshift space, where the “Finger of God” effect can introduce some spurious filaments in dense groups and clusters. The FoG effects primarily distort structures on smaller scales (e.g., groups and some clusters), while the large-scale density field remains relatively unaffected. We smooth the density field on grids using a Gaussian Filter of width 8 Mpc. This implies that our study focuses on large-scale environments where the impact of FoGs should be minimal. Our volume limited sample also do not contain very high density groups and clusters due to the spectroscopic incompleteness arising from the finite size of the SDSS fibres and the fibre collisions. Our main emphasis lies in exploring the impact of the large-scale geometric environments in the cosmic web on the interrelationships between various galaxy properties. We do not expect FoGs to bias our measurements of the large-scale environment due to these reasons. Further, the observed trends in PC1, PC2 and PC3 might reflect a combination of local and global influences, as local density naturally correlates with the global cosmic web structure. So the differences observed in our analysis is a combined outcome of the local density of galaxies and the large-scale cosmic web environment. We tried to repeat our analysis by simultaneously matching the stellar mass and the local density in all types of cosmic web environments. Unfortunately, this provides us with a small number of galaxies which represent only the lowest density regions from each type of cosmic web environment.

Finally, our study demonstrates that PCA provides a powerful tool for dissecting the impacts of the cosmic web on

galaxy evolution. The results highlight the complementary roles of external environmental effects and internal secular processes in shaping galaxy properties and their correlations.

## ACKNOWLEDGEMENT

Authors thank the anonymous reviewers for the valuable comments and suggestions that helped us to improve the draft. AN acknowledges the financial support from the Department of Science and Technology (DST), Government of India through an INSPIRE fellowship. BP would like to acknowledge financial support from the SERB, DST, Government of India through the project CRG/2019/001110. BP would also like to acknowledge IUCAA, Pune, for providing support through the associateship programme.

We would also like to acknowledge the use of several Python packages such as Pandas (McKinney, 2010), NumPy (Harris et al., 2020), SciPy (Virtanen et al., 2020) and Matplotlib (Hunter, 2007) in our work.

Funding for the SDSS and SDSS-II has been provided by the Alfred P. Sloan Foundation, the Participating Institutions, the National Science Foundation, the U.S. Department of Energy, the National Aeronautics and Space Administration, the Japanese Monbukagakusho, the Max Planck Society, and the Higher Education Funding Council for England. The SDSS website is <http://www.sdss.org/>.

The SDSS is managed by the Astrophysical Research Consortium for the Participating Institutions. The Participating Institutions are the American Museum of Natural History, Astrophysical Institute Potsdam, University of Basel, University of Cambridge, Case Western Reserve University, University of Chicago, Drexel University, Fermilab, the Institute for Advanced Study, the Japan Participation Group, Johns Hopkins University, the Joint Institute for Nuclear Astrophysics, the Kavli Institute for Particle Astrophysics and Cosmology, the Korean Scientist Group, the Chinese Academy of Sciences (LAMOST), Los Alamos National Laboratory, the Max-Planck-Institute for Astronomy (MPIA), the Max-Planck-Institute for Astrophysics (MPA), New Mexico State University, Ohio State University, University of Pittsburgh, University of Portsmouth, Princeton University, the United States Naval Observatory, and the University of Washington.

## References

- M. J. Rees and J. P. Ostriker. Cooling, dynamics and fragmentation of massive gas clouds: clues to the masses and radii of galaxies and clusters. *MNRAS*, 179:541–559, June 1977. doi: 10.1093/mnras/179.4.541.
- J. Silk. On the fragmentation of cosmic gas clouds. I. The formation of galaxies and the first generation of stars. *ApJ*, 211:638–648, February 1977. doi: 10.1086/154972.
- Simon D. M. White and M. J. Rees. Core condensation in heavy halos: A Two stage theory for galaxy formation and clusters. *Mon. Not. Roy. Astron. Soc.*, 183:341–358, 1978. doi: 10.1093/mnras/183.3.341.
- S. M. Fall and G. Efstathiou. Formation and rotation of disc galaxies with haloes. *MNRAS*, 193:189–206, October 1980. doi: 10.1093/mnras/193.2.189.
- Marc Davis and Margaret J. Geller. Galaxy Correlations as a Function of Morphological Type. *ApJ*, 208:13–19, August 1976. doi: 10.1086/154575.
- A. Dressler. Galaxy morphology in rich clusters: Implications for the formation and evolution of galaxies. *Astrophys. J.*, 236:351–365, 1980. doi: 10.1086/157753.
- H. R. Butcher and A. Oemler, Jr. Nature, of blue galaxies in the cluster CL 1447+2619. *Nature*, 310:31–33, July 1984. doi: 10.1038/310031a0.
- Luigi Guzzo, Michael A. Strauss, Karl B. Fisher, Riccardo Giovanelli, and Martha P. Haynes. Redshift-space distortions and the real-space clustering of different galaxy types. *Astrophys. J.*, 489:37–48, 1997. doi: 10.1086/304788.
- I. Zehavi et al. Galaxy Clustering in early SDSS Redshift Data. *Astrophys. J.*, 571:172–190, 2002. doi: 10.1086/339893.
- Tomotsugu Goto, Chisato Yamauchi, Yutaka Fujita, Sadanori Okamura, Maki Sekiguchi, Ian Smail, Mariangela Bernardi, and Percy L. Gomez. The morphology-density relation in the Sloan Digital Sky Survey. *MNRAS*, 346(2):601–614, December 2003. doi: 10.1046/j.1365-2966.2003.07114.x.
- David W. Hogg et al. The Overdensities of Galaxy Environments as a Function of Luminosity and Color. *Astrophys. J. Lett.*, 585:L5–L10, 2003. doi: 10.1086/374238.
- Michael R. Blanton et al. The Broad - band optical properties of galaxies with redshifts  $0.0 < z < 0.2$ . *Astrophys. J.*, 594:186, 2003. doi: 10.1086/375528.
- J. Einasto, G. Hutsi, M. Einasto, E. Saar, D. L. Tucker, V. Muller, P. Heinamaki, and S. S. Allam. Clusters and Superclusters in the Sloan Digital Sky Survey. *Astron. Astrophys.*, 405:425–444, 2003. doi: 10.1051/0004-6361:20030419.
- Michael Balogh, Ian Smail, R. Bower, B. Ziegler, G. Smith, R. Davies, A. Gaztelu, J. P. Kneib, and H. Ebeling. Distinguishing local and global influences on galaxy morphology: an hst comparison of high and low x-ray luminosity clusters. *Astrophys. J.*, 566:123, 2002. doi: 10.1086/338056.
- Guinevere Kauffmann, Simon D. M. White, Timothy M. Heckman, Brice Menard, Jarle Brinchmann, Stephane Charlot, Christy Tremonti, and Jon Brinkmann. The Environmental dependence of the relations between stellar mass, structure, star formation and nuclear activity in galaxies. *Mon. Not. Roy. Astron. Soc.*, 353:713–731, 2004. doi: 10.1111/j.1365-2966.2004.08117.x.

- Rachel Mandelbaum, Uros Seljak, Guinevere Kauffmann, Christopher M. Hirata, and Jonathan Brinkmann. Galaxy halo masses and satellite fractions from galaxy-galaxy lensing in the sdss: stellar mass, luminosity, morphology, and environment dependencies. *Mon. Not. Roy. Astron. Soc.*, 368:715, 2006. doi: 10.1111/j.1365-2966.2006.10156.x.
- Umami Abbas and Ravi K. Sheth. The environmental dependence of galaxy clustering in the sloan digital sky survey. *Mon. Not. Roy. Astron. Soc.*, 372:1749–1754, 2006. doi: 10.1111/j.1365-2966.2006.10987.x.
- Biswajit Pandey and Somnath Bharadwaj. The luminosity bias relation from filaments in the Sloan Digital Sky Survey Data Release Four. *Mon. Not. Roy. Astron. Soc.*, 377:L15–L19, 2007. doi: 10.1111/j.1745-3933.2007.00294.x.
- M. Mouhcine, I. K. Baldry, and Steven Peter Bamford. The environmental dependence of the chemical properties of star-forming galaxies. *Mon. Not. Roy. Astron. Soc.*, 382:801–808, 2007. doi: 10.1111/j.1365-2966.2007.12405.x.
- Steven P. Bamford et al. Galaxy Zoo: the independence of morphology and colour. *Mon. Not. Roy. Astron. Soc.*, 393:1324–1352, 2009. doi: 10.1111/j.1365-2966.2008.14252.x.
- Michael C. Cooper, Anna Gallazzi, Jeffrey A. Newman, and Renbin Yan. Galaxy assembly bias on the red sequence. *MNRAS*, 402(3):1942–1958, March 2010. doi: 10.1111/j.1365-2966.2009.16020.x.
- Yusei Koyama et al. On the evolution and environmental dependence of the star formation rate versus stellar mass relation since  $z^2$ . *Mon. Not. Roy. Astron. Soc.*, 434:423, 2013. doi: 10.1093/mnras/stt1035.
- Alar Toomre and Juri Toomre. Galactic Bridges and Tails. *ApJ*, 178:623–666, December 1972. doi: 10.1086/151823.
- Joshua E. Barnes and Lars Hernquist. Transformations of Galaxies. II. Gasdynamics in Merging Disk Galaxies. *ApJ*, 471:115, November 1996. doi: 10.1086/177957.
- J. Christopher Mihos and Lars Hernquist. Gasdynamics and Starbursts in Major Mergers. *ApJ*, 464:641, June 1996. doi: 10.1086/177353.
- P. B. Tissera, R. Domínguez-Tenreiro, C. Scannapieco, and A. Sáiz. Double starbursts triggered by mergers in hierarchical clustering scenarios. *MNRAS*, 333(2):327–338, June 2002. doi: 10.1046/j.1365-8711.2002.05385.x.
- T. J. Cox, Patrik Jonsson, Joel R. Primack, and Rachel S. Somerville. Feedback in simulations of disc-galaxy major mergers. *MNRAS*, 373(3):1013–1038, December 2006. doi: 10.1111/j.1365-2966.2006.11107.x.
- M. Montuori, P. Di Matteo, M. D. Lehnert, F. Combes, and B. Semelin. The dilution peak, metallicity evolution, and dating of galaxy interactions and mergers. *A&A*, 518:A56, July 2010. doi: 10.1051/0004-6361/201014304.
- Jennifer M. Lotz, Patrik Jonsson, T. J. Cox, Darren Croton, Joel R. Primack, Rachel S. Somerville, and Kyle Stewart. The Major and Minor Galaxy Merger Rates at  $z \lesssim 1.5$ . *ApJ*, 742(2):103, December 2011. doi: 10.1088/0004-637X/742/2/103.
- Paul Torrey, T. J. Cox, Lisa Kewley, and Lars Hernquist. The Metallicity Evolution of Interacting Galaxies. *ApJ*, 746(1):108, February 2012. doi: 10.1088/0004-637X/746/1/108.
- Philip F. Hopkins, Thomas J. Cox, Lars Hernquist, Desika Narayanan, Christopher C. Hayward, and Norman Murray. Star formation in galaxy mergers with realistic models of stellar feedback and the interstellar medium. *MNRAS*, 430(3):1901–1927, April 2013. doi: 10.1093/mnras/stt017.
- F. Renaud, F. Bounaud, K. Kraljic, and P. A. Duc. Starbursts triggered by intergalactic tides and interstellar compressive turbulence. *MNRAS*, 442:L33–L37, July 2014. doi: 10.1093/mnras/flu050.
- Florent Renaud, Frédéric Bounaud, and Pierre-Alain Duc. A parsec-resolution simulation of the Antennae galaxies: formation of star clusters during the merger. *MNRAS*, 446(2):2038–2054, January 2015. doi: 10.1093/mnras/stu2208.
- Jorge Moreno, Paul Torrey, Sara L. Ellison, David R. Patton, Asa F. L. Bluck, Gunjan Bansal, and Lars Hernquist. Mapping galaxy encounters in numerical simulations: the spatial extent of induced star formation. *MNRAS*, 448(2):1107–1117, April 2015. doi: 10.1093/mnras/stv094.
- Jorge Moreno, Paul Torrey, Sara L. Ellison, David R. Patton, Connor Bottrell, Asa F. L. Bluck, Maan H. Hani, Christopher C. Hayward, James S. Bullock, Philip F. Hopkins, and Lars Hernquist. Spatially resolved star formation and fuelling in galaxy interactions. *MNRAS*, 503(3):3113–3133, May 2021. doi: 10.1093/mnras/staa2952.
- Florent Renaud, Álvaro Segovia Otero, and Oscar Agertz. The merger-starburst connection across cosmic times. *MNRAS*, 516(4):4922–4931, November 2022. doi: 10.1093/mnras/stac2557.
- Apashanka Das and Biswajit Pandey. The roles of environment and interactions on the evolution of red and blue galaxies in the EAGLE simulation. *JCAP*, 2024(8):060, August 2024. doi: 10.1088/1475-7516/2024/08/060.
- R. B. Larson and B. M. Tinsley. Star formation rates in normal and peculiar galaxies. *ApJ*, 219:46–59, January 1978. doi: 10.1086/155753.
- Elizabeth J. Barton, Margaret J. Geller, and Scott J. Kenyon. Tidally Triggered Star Formation in Close Pairs of Galaxies. *ApJ*, 530(2):660–679, February 2000. doi: 10.1086/308392.
- Diego G. Lambas, Patricia B. Tissera, M. Sol Alonso, and Georgina Coldwell. Galaxy pairs in the 2dF survey - I. Effects of interactions on star formation in the field. *MNRAS*, 346(4):1189–1196, December 2003. doi: 10.1111/j.1365-2966.2003.07179.x.
- M. Sol Alonso, Patricia B. Tissera, Georgina Coldwell, and Diego G. Lambas. Galaxy pairs in the 2dF survey - II. Effects of interactions on star formation in groups and clusters. *MNRAS*, 352(3):1081–1088, August 2004. doi: 10.1111/j.1365-2966.2004.08002.x.
- B. Nikolic, H. Cullen, and P. Alexander. Star formation in close pairs selected from the Sloan Digital Sky Survey. *MNRAS*, 355(3):874–886, December 2004. doi: 10.1111/j.1365-2966.2004.08366.x.
- Deborah Freedman Woods, Margaret J. Geller, and Elizabeth J. Barton. Tidally Triggered Star Formation in Close Pairs of Galaxies: Major and Minor Interactions. *AJ*, 132(1):197–209, July 2006. doi: 10.1086/504834.
- Deborah Freedman Woods and Margaret J. Geller. Minor Galaxy Interactions: Star Formation Rates and Galaxy Properties. *AJ*, 134(2):527–540, August 2007. doi: 10.1086/519381.
- Elizabeth J. Barton, Jacob A. Arnold, Andrew R. Zentner, James S. Bullock, and Risa H. Wechsler. Isolating Triggered Star Formation. *ApJ*, 671(2):1538–1549, December 2007. doi: 10.1086/522620.
- Sara L. Ellison, David R. Patton, Luc Simard, and Alan W. McConnachie. Galaxy Pairs in the Sloan Digital Sky Survey I: Star Formation, AGN Fraction, and the Luminosity/Mass-Metallicity Relation. *Astron. J.*, 135:1877, 2008. doi: 10.1088/0004-6256/135/5/1877.
- Sara L. Ellison, David R. Patton, Luc Simard, Alan W. McConnachie, Ivan K. Baldry, and J. Trevor Mendel. Galaxy pairs in the Sloan Digital Sky Survey - II. The effect of environment on interactions. *MNRAS*, 407(3):1514–1528, September 2010. doi: 10.1111/j.1365-2966.2010.17076.x.
- Deborah Freedman Woods, Margaret J. Geller, Michael J. Kurtz, Eduard Westra, Daniel G. Fabricant, and Ian Dell’Antonio. Triggered Star



- Formation in Galaxy Pairs at  $z = 0.08\text{--}0.38$ . *AJ*, 139(5):1857–1870, May 2010. doi: 10.1088/0004-6256/139/5/1857.
- David R. Patton, Sara L. Ellison, Luc Simard, Alan W. McConnachie, and J. Trevor Mendel. Galaxy pairs in the Sloan Digital Sky Survey - III. Evidence of induced star formation from optical colours. *MNRAS*, 412(1):591–606, March 2011. doi: 10.1111/j.1365-2966.2010.17932.x.
- J. K. Barrera-Ballesteros, S. F. Sánchez, B. García-Lorenzo, J. Falcón-Barroso, D. Mast, R. García-Benito, B. Husemann, G. van de Ven, J. Iglesias-Páramo, F. F. Rosales-Ortega, M. A. Pérez-Torres, I. Márquez, C. Kehrig, R. A. Marino, J. M. Vilchez, L. Galbany, Á. R. López-Sánchez, C. J. Walcher, and CALIFA Collaboration. Central star formation and metallicity in CALIFA interacting galaxies. *A&A*, 579:A45, July 2015. doi: 10.1051/0004-6361/201425397.
- Mallory D. Thorp, Sara L. Ellison, Hsi-An Pan, Lihwai Lin, David R. Patton, Asa F. L. Bluck, Dan Walters, and Jillian M. Scudder. The almaquest survey x: What powers merger induced star formation? *Monthly Notices of the Royal Astronomical Society*, 2022. URL <https://api.semanticscholar.org/CorpusID:251564682>.
- Ekta A. Shah, Jeyhan S. Kartaltepe, Christina T. Magagnoli, Isabella G. Cox, Caleb T. Wetherell, Brittany N. Vanderhoof, Kevin C. Cooke, Antonello Calabro, Nima Chartab, Christopher J. Conselice, Darren J. Croton, Alexander de la Vega, Nimish P. Hathi, Olivier Ilbert, Hanae Inami, Dale D. Kocevski, Anton M. Koekemoer, Brian C. Lemaux, Lori Lubin, Kameswara Bharadwaj Mantha, Stefano Marchesi, Marie Martig, Jorge Moreno, Belen Alcalde Pampiega, David R. Patton, Mara Salvato, and Ezequiel Treister. Investigating the Effect of Galaxy Interactions on Star Formation at  $0.5 < z < 3.0$ . *ApJ*, 940(1):4, November 2022. doi: 10.3847/1538-4357/ac96eb.
- Apashanka Das, Biswajit Pandey, and Suman Sarkar. Galaxy Interactions in Filaments and Sheets: Effects of the Large-scale Structures Versus the Local Density. *Res. Astron. Astrophys.*, 23(2):025016, 2023. doi: 10.1088/1674-4527/acab44.
- Philip F. Hopkins, Lars Hernquist, Thomas J. Cox, and Dušan Kereš. A Cosmological Framework for the Co-Evolution of Quasars, Supermassive Black Holes, and Elliptical Galaxies. I. Galaxy Mergers and Quasar Activity. *ApJS*, 175(2):356–389, April 2008. doi: 10.1086/524362.
- Ben Moore, Neal Katz, George Lake, Alan Dressler, and Augustus Oemler. Galaxy harassment and the evolution of clusters of galaxies. *Nature*, 379(6566):613–616, February 1996. doi: 10.1038/379613a0.
- Ben Moore, George Lake, and Neal Katz. Morphological Transformation from Galaxy Harassment. *ApJ*, 495(1):139–151, March 1998. doi: 10.1086/305264.
- James E. Gunn and J. Richard Gott, III. On the Infall of Matter Into Clusters of Galaxies and Some Effects on Their Evolution. *ApJ*, 176:1, August 1972. doi: 10.1086/151605.
- Michael L. Balogh, Julio F. Navarro, and Simon L. Morris. The Origin of Star Formation Gradients in Rich Galaxy Clusters. *ApJ*, 540(1):113–121, September 2000. doi: 10.1086/309323.
- R. B. Larson, B. M. Tinsley, and C. N. Caldwell. The evolution of disk galaxies and the origin of S0 galaxies. *Astrophys. J.*, 237:692–707, 1980. doi: 10.1086/157917.
- Rachel S. Somerville and Joel R. Primack. Semi-analytic modelling of galaxy formation: the local Universe. *MNRAS*, 310(4):1087–1110, December 1999. doi: 10.1046/j.1365-8711.1999.03032.x.
- Daisuke Kawata and John S. Mulchaey. Strangulation in Galaxy Groups. *ApJ Letters*, 672(2):L103, January 2008. doi: 10.1086/526544.
- M. Geha, M. R. Blanton, R. Yan, and J. L. Tinker. A Stellar Mass Threshold for Quenching of Field Galaxies. *ApJ*, 757(1):85, September 2012. doi: 10.1088/0004-637X/757/1/85.
- Yuval Birnboim and Avishai Dekel. Virial shocks in galactic haloes? *MNRAS*, 345(1):349–364, October 2003. doi: 10.1046/j.1365-8711.2003.06955.x.
- Avishai Dekel and Yuval Birnboim. Galaxy bimodality due to cold flows and shock heating. *MNRAS*, 368(1):2–20, May 2006. doi: 10.1111/j.1365-2966.2006.10145.x.
- Dušan Kereš, Neal Katz, David H. Weinberg, and Romeel Davé. How do galaxies get their gas? *MNRAS*, 363(1):2–28, October 2005. doi: 10.1111/j.1365-2966.2005.09451.x.
- J. M. Gabor, R. Davé, K. Finlator, and B. D. Oppenheimer. How is star formation quenched in massive galaxies? *MNRAS*, 407(2):749–771, September 2010. doi: 10.1111/j.1365-2966.2010.16961.x.
- Marie Martig, Frédéric Bournaud, Romain Teyssier, and Avishai Dekel. Morphological Quenching of Star Formation: Making Early-Type Galaxies Red. *ApJ*, 707(1):250–267, December 2009. doi: 10.1088/0004-637X/707/1/250.
- Karen L. Masters, Moein Mosleh, A. Kathy Romer, Robert C. Nichol, Steven P. Bamford, Kevin Schawinski, Chris J. Lintott, Dan Andreescu, Heather C. Campbell, Ben Crowcroft, Isabelle Doyle, Edward M. Edmondson, Phil Murray, M. Jordan Raddick, Anže Slosar, Alexander S. Szalay, and Jan Vandenberg. Galaxy Zoo: passive red spirals. *MNRAS*, 405(2):783–799, June 2010. doi: 10.1111/j.1365-2966.2010.16503.x.
- Ying-jie Peng and Alvio Renzini. Disc growth and quenching. *MNRAS*, 491(1):L51–L55, January 2020. doi: 10.1093/mnras/slz163.
- S. A. Gregory and L. A. Thompson. The Coma/A1367 supercluster and its environs. *ApJ*, 222:784–799, June 1978. doi: 10.1086/156198.
- Mihkel Jõeveer and Jaan Einasto. Has the universe the cell structure? In *Symposium-International Astronomical Union*, volume 79, pages 241–251. Cambridge University Press, 1978.
- Jaan Einasto, Mihkel Jõeveer, and Enn Saar. Structure of superclusters and supercluster formation. *Monthly Notices of the Royal Astronomical Society*, 193(2):353–375, 11 1980. ISSN 0035-8711. doi: 10.1093/mnras/193.2.353. URL <https://doi.org/10.1093/mnras/193.2.353>.
- Ia. B. Zeldovich and S. F. Shandarin. “Black” regions in the universe. *Pisma v Astronomicheskii Zhurnal*, 8:131–135, April 1982.
- J. Einasto, A. A. Klypin, E. Saar, and S. F. Shandarin. Structure of superclusters and supercluster formation - III. Quantitative study of the Local Supercluster. *MNRAS*, 206:529–558, February 1984. doi: 10.1093/mnras/206.3.529.
- J. Richard Bond, Lev Kofman, and Dmitry Pogosyan. How filaments of galaxies are woven into the cosmic web. *Nature*, 380(6575):603–606, April 1996. doi: 10.1038/380603a0.
- Somnath Bharadwaj, Varun Sahni, B. S. Sathyaprakash, Sergei F. Shandarin, and Capp Yess. Evidence for Filamentarity in the Las Campanas Redshift Survey. *ApJ*, 528(1):21–29, January 2000. doi: 10.1086/308163.
- Biswajit Pandey and Somnath Bharadwaj. A two-dimensional analysis of percolation and filamentarity in the Sloan Digital Sky Survey Data Release One. *MNRAS*, 357(3):1068–1076, March 2005. doi: 10.1111/j.1365-2966.2005.08726.x.
- Miguel A. Aragón-Calvo, Rien van de Weygaert, and Bernard J. T. Jones. Multiscale phenomenology of the cosmic web. *Monthly Notices of the Royal Astronomical Society*, 408(4):2163–2187, 10 2010. ISSN 0035-8711. doi: 10.1111/j.1365-2966.2010.17263.x. URL <https://doi.org/10.1111/j.1365-2966.2010.17263.x>.

- Noam I. Libeskind, Rien van de Weygaert, Marius Cautun, Bridget Falck, Elmo Tempel, Tom Abel, Mehmet Alpaslan, Miguel A. Aragón-Calvo, Jaime E. Forero-Romero, Roberto Gonzalez, Stefan Gottlöber, Oliver Hahn, Wojciech A. Hellwing, Yehuda Hoffman, Bernard J. T. Jones, Francisco Kitaura, Alexander Knebe, Serena Manti, Mark Neyrinck, Sebastián E. Nuza, Nelson Padilla, Erwin Platen, Nesar Ramachandra, Aaron Robotham, Enn Saar, Sergei Shandarin, Matthias Steinmetz, Radu S. Stoica, Thierry Sousbie, and Gustavo Yepes. Tracing the cosmic web. *Monthly Notices of the Royal Astronomical Society*, 473(1):1195–1217, 08 2017. ISSN 0035-8711. doi: 10.1093/mnras/stx1976. URL <https://doi.org/10.1093/mnras/stx1976>.
- Miguel A. Aragón-Calvo, Erwin Platen, Rien van de Weygaert, and Alexander S. Szalay. The Spine of the Cosmic Web. *ApJ*, 723(1):364–382, November 2010. doi: 10.1088/0004-637X/723/1/364.
- Marius Cautun, Rien van de Weygaert, Bernard J. T. Jones, and Carlos S. Frenk. Evolution of the cosmic web. *MNRAS*, 441(4):2923–2973, July 2014. doi: 10.1093/mnras/stu768.
- Nesar S. Ramachandra and Sergei F. Shandarin. Multi-stream portrait of the cosmic web. *MNRAS*, 452(2):1643–1653, September 2015. doi: 10.1093/mnras/stv1389.
- Wei Wang, Peng Wang, Hong Guo, Xi Kang, Noam I. Libeskind, Daniela Galárraga-Espinosa, Volker Springel, Rahul Kannan, Lars Hernquist, Rüdiger Pakmor, Hao-Ran Yu, Sownak Bose, Quan Guo, Luo Yu, and César Hernández-Aguayo. The boundary of cosmic filaments. *MNRAS*, 532(4):4604–4615, August 2024. doi: 10.1093/mnras/stae1801.
- T. Tuominen, J. Nevalainen, E. Tempel, T. Kuutma, N. Wijers, J. Schaye, P. Heinämäki, M. Bonamente, and P. Ganeshaiah Veena. An EAGLE view of the missing baryons. *A&A*, 646:A156, February 2021. doi: 10.1051/0004-6361/202039221.
- Daniela Galárraga-Espinosa, Nabila Aghanim, Mathieu Langer, and Hideki Tanimura. Properties of gas phases around cosmic filaments at  $z = 0$  in the IllustrisTNG simulation. *A&A*, 649:A117, May 2021. doi: 10.1051/0004-6361/202039781.
- Nicolas Cornuault, Matthew Lehnert, François Boulanger, and Pierre Guillard. Are Cosmological Gas Accretion Streams Multiphase and Turbulent? *arXiv e-prints*, art. arXiv:1609.04405, September 2016. doi: 10.48550/arXiv.1609.04405.
- Weishan Zhu, Fupeng Zhang, and Long-Long Feng. Impact of Cosmic Filaments on the Gas Accretion Rate of Dark Matter Halos. *ApJ*, 924(2):132, January 2022. doi: 10.3847/1538-4357/ac37b9.
- Yen-Chi Chen, Shirley Ho, Rachel Mandelbaum, Neta A. Bahcall, Joel R. Brownstein, Peter E. Freeman, Christopher R. Genovese, Donald P. Schneider, and Larry Wasserman. Detecting effects of filaments on galaxy properties in the Sloan Digital Sky Survey III. *MNRAS*, 466(2):1880–1893, April 2017a. doi: 10.1093/mnras/stw3127.
- Biswajit Pandey and Suman Sarkar. Exploring galaxy colour in different environments of the cosmic web with SDSS. *MNRAS*, 498(4):6069–6082, November 2020. doi: 10.1093/mnras/staa2772.
- Ankit Singh, Smriti Mahajan, and Jasjeet Singh Bagla. Study of galaxies on large-scale filaments in simulations. *MNRAS*, 497(2):2265–2275, September 2020. doi: 10.1093/mnras/staa1913.
- C. Laigle, C. Pichon, S. Codis, Y. Dubois, D. Le Borgne, D. Pogossyan, J. Devriendt, S. Peirani, S. Prunet, S. Rouberol, A. Slyz, and T. Sousbie. Swirling around filaments: are large-scale structure vortices spinning up dark haloes? *MNRAS*, 446(3):2744–2759, January 2015. doi: 10.1093/mnras/stu2289.
- Apashanka Das, Biswajit Pandey, and Suman Sarkar. Do Minor Interactions Trigger Star Formation in Galaxy Pairs? *Research in Astronomy and Astrophysics*, 23(9):095026, September 2023. doi: 10.1088/1674-4527/aceccb.
- Munira Hoosain, Sarah-L. Blyth, Rosalind E. Skelton, Sheila J. Kannappan, David V. Stark, Kathleen D. Eckert, Zackary L. Hutchens, Derrick S. Carr, and Katarina Kraljic. The effect of cosmic web filaments on galaxy properties in the RESOLVE and ECO surveys. *MNRAS*, 528(3):4139–4159, March 2024. doi: 10.1093/mnras/stae174.
- Teodora-Elena Bulichi, Romeel Davé, and Katarina Kraljic. How galaxy properties vary with filament proximity in the SIMBA simulations. *MNRAS*, 529(3):2595–2610, April 2024. doi: 10.1093/mnras/stae667.
- Romeel Davé, Daniel Anglés-Alcázar, Desika Narayanan, Qi Li, Mika H. Rafieferantsoa, and Sarah Appleby. SIMBA: Cosmological simulations with black hole growth and feedback. *MNRAS*, 486(2):2827–2849, June 2019. doi: 10.1093/mnras/stz937.
- Farhanul Hasan, Joseph N. Burchett, Douglas Hellinger, Oskar Elek, Daisuke Nagai, S. M. Faber, Joel R. Primack, David C. Koo, Nir Mandelker, and Joanna Woo. Filaments of the Slime Mold Cosmic Web and How They Affect Galaxy Evolution. *ApJ*, 970(2):177, August 2024. doi: 10.3847/1538-4357/ad4ee2.
- Dylan Nelson, Volker Springel, Annalisa Pillepich, Vicente Rodriguez-Gomez, Paul Torrey, Shy Genel, Mark Vogelsberger, Ruediger Pakmor, Federico Marinacci, Rainer Weinberger, Luke Kelley, Mark Lovell, Benedikt Diemer, and Lars Hernquist. The IllustrisTNG simulations: public data release. *Computational Astrophysics and Cosmology*, 6(1):2, May 2019. doi: 10.1186/s40668-019-0028-x.
- Tommaso Treu, Richard S. Ellis, Jean-Paul Kneib, Alan Dressler, Ian Smail, Oliver Czoske, Augustus Oemler, and Priyamvada Natarajan. A Wide-Field Hubble Space Telescope Study of the Cluster Cl 0024+16 at  $z = 0.4$ . I. Morphological Distributions to 5 Mpc Radius. *ApJ*, 591(1):53–78, July 2003. doi: 10.1086/375314.
- Gabriella De Lucia, Simone Weinmann, Bianca M. Poggianti, Alfonso Aragón-Salamanca, and Dennis Zaritsky. The environmental history of group and cluster galaxies in a  $\Lambda$  cold dark matter universe. *MNRAS*, 423(2):1277–1292, June 2012. doi: 10.1111/j.1365-2966.2012.20983.x.
- Callum T. Donnan, Rita Tojeiro, and Katarina Kraljic. The role of the cosmic web in the scatter of the galaxy stellar mass-gas metallicity relation. *Nature Astronomy*, 6:599–606, March 2022. doi: 10.1038/s41550-022-01619-w.
- Maret Einasto, Rain Kipper, Peeter Tenjes, Jaan Einasto, Elmo Tempel, and Lauri Juhan Liivamägi. Death at watersheds: Galaxy quenching in low-density environments. *A&A*, 668:A69, December 2022. doi: 10.1051/0004-6361/202244304.
- Agustín M. Rodríguez-Medrano, Volker Springel, Federico A. Stasyszyn, and Dante J. Paz. The evolutionary path of void galaxies in TNG300 simulation. *MNRAS*, 528(2):2822–2833, February 2024. doi: 10.1093/mnras/stae193.
- Idit Zehavi, Zheng Zheng, David H. Weinberg, Michael R. Blanton, Neta A. Bahcall, Andreas A. Berlind, Jon Brinkmann, Joshua A. Frieman, James E. Gunn, Robert H. Lupton, Robert C. Nichol, Will J. Percival, Donald P. Schneider, Ramin A. Skibba, Michael A. Strauss, Max Tegmark, and Donald G. York. Galaxy Clustering in the Completed SDSS Redshift Survey: The Dependence on Color and Luminosity. *ApJ*, 736(1):59, July 2011. doi: 10.1088/0004-637X/736/1/59.
- Helming Yan, Zuhui Fan, and Simon D. M. White. The dependence of galaxy properties on the large-scale tidal environment. *Monthly Notices of the Royal Astronomical Society*, 430(4):3432–3444, 02 2013. ISSN 0035-8711. doi: 10.1093/mnras/stt141. URL <https://doi.org/10.1093/mnras/stt141>.

- mnras/stt141*.
- Mehmet Alpaslan, Simon Driver, Aaron S. G. Robotham, Danail Obreschkow, Ellen Andrae, Michelle Cluver, Lee S. Kelvin, Rebecca Lange, Matt Owers, Edward N. Taylor, Stephen K. Andrews, Steven Bamford, Joss Bland-Hawthorn, Sarah Brough, Michael J. I. Brown, Matthew Colless, Luke J. M. Davies, Elizabeth Eardley, Meiart W. Grootes, Andrew M. Hopkins, Rebecca Kennedy, Jochen Liske, Maritza A. Lara-López, Ángel R. López-Sánchez, Jon Loveday, Barry F. Madore, Smriti Mahajan, Martin Meyer, Amanda Moffett, Peder Norberg, Samantha Penny, Kevin A. Pimbblet, Cristina C. Popescu, Mark Seibert, and Richard Tuffs. Galaxy And Mass Assembly (GAMA): trends in galaxy colours, morphology, and stellar populations with large-scale structure, group, and pair environments. *MNRAS*, 451(3):3249–3268, August 2015. doi: 10.1093/mnras/stv1176.
- Shadab Alam, Ying Zu, John A. Peacock, and Rachel Mandelbaum. Cosmic web dependence of galaxy clustering and quenching in SDSS. *MNRAS*, 483(4):4501–4517, March 2019. doi: 10.1093/mnras/sty3477.
- Biswajit Pandey and Somnath Bharadwaj. The luminosity, colour and morphology dependence of galaxy filaments in the Sloan Digital Sky Survey Data Release Four. *MNRAS*, 372(2):827–838, October 2006. doi: 10.1111/j.1365-2966.2006.10894.x.
- Biswajit Pandey and Somnath Bharadwaj. Exploring star formation using the filaments in the Sloan Digital Sky Survey Data Release Five. *MNRAS*, 387(2):767–771, June 2008. doi: 10.1111/j.1365-2966.2008.13262.x.
- Ignacio Trujillo, Conrado Carretero, and Santiago G. Patiri. Detection of the effect of cosmological large-scale structure on the orientation of galaxies. *Astrophys. J. Lett.*, 640:L111–L114, 2006. doi: 10.1086/503548.
- Jounghun Lee and Pirin Erdogdu. The Alignments of the Galaxy Spins with the Real-Space Tidal Field Reconstructed from the 2MASS Redshift Survey. *ApJ*, 671(2):1248–1255, December 2007. doi: 10.1086/523351.
- Dante J. Paz, Federico Stasyszyn, and Nelson D. Padilla. Angular momentum-large-scale structure alignments in  $\Lambda$ CDM models and the SDSS. *MNRAS*, 389(3):1127–1136, September 2008. doi: 10.1111/j.1365-2966.2008.13655.x.
- Bernard J. T. Jones, Rien van de Weygaert, and Miguel A. Aragón-Calvo. Fossil evidence for spin alignment of Sloan Digital Sky Survey galaxies in filaments. *MNRAS*, 408(2):897–918, October 2010. doi: 10.1111/j.1365-2966.2010.17202.x.
- Jillian M. Scudder, Sara L. Ellison, and J. Trevor Mendel. The dependence of galaxy group star formation rates and metallicities on large-scale environment. *MNRAS*, 423(3):2690–2704, July 2012. doi: 10.1111/j.1365-2966.2012.21080.x.
- Elmo Tempel and Noam I. Libeskind. Galaxy spin alignment in filaments and sheets: observational evidence. *Astrophys. J. Lett.*, 775:L42, 2013. doi: 10.1088/2041-8205/775/2/L42.
- E. Tempel, R. S. Stoica, and E. Saar. Evidence for spin alignment of spiral and elliptical/S0 galaxies in filaments. *MNRAS*, 428(2):1827–1836, January 2013. doi: 10.1093/mnras/sts162.
- B. Darvish, D. Sobral, B. Mobasher, N. Z. Scoville, P. Best, L. V. Sales, and I. Smail. Cosmic Web and Star Formation Activity in Galaxies at  $z \sim 1$ . *ApJ*, 796(1):51, November 2014. doi: 10.1088/0004-637X/796/1/51.
- M. E. Filho, J. Sánchez Almeida, C. Muñoz-Tuñón, S. E. Nuza, F. Kitaura, and S. Heß. Extremely Metal-poor Galaxies: The Environment. *ApJ*, 802(2):82, April 2015. doi: 10.1088/0004-637X/802/2/82.
- H. E. Luparello, M. Lares, D. Paz, C. Y. Yaryura, D. G. Lambas, and N. Padilla. Brightest group galaxies and the large-scale environment. *MNRAS*, 448(2):1483–1493, April 2015. doi: 10.1093/mnras/stv082.
- Mehmet Alpaslan, Meiart Grootes, Pamela M. Marcum, Cristina Popescu, Richard Tuffs, Joss Bland-Hawthorn, Sarah Brough, Michael J. I. Brown, Luke J. M. Davies, Simon P. Driver, Benne W. Holwerda, Lee S. Kelvin, Maritza A. Lara-López, Ángel R. López-Sánchez, Jon Loveday, Amanda Moffett, Edward N. Taylor, Matt Owers, and Aaron S. G. Robotham. Galaxy And Mass Assembly (GAMA): stellar mass growth of spiral galaxies in the cosmic web. *MNRAS*, 457(3):2287–2300, April 2016. doi: 10.1093/mnras/stw134.
- Biswajit Pandey and Suman Sarkar. How much a galaxy knows about its large-scale environment?: An information theoretic perspective. *MNRAS*, 467(1):L6–L10, May 2017. doi: 10.1093/mnras/slz250.
- Teet Kuutma, Antti Tamm, and Elmo Tempel. From voids to filaments: environmental transformations of galaxies in the SDSS. *A&A*, 600:L6, April 2017. doi: 10.1051/0004-6361/201730526.
- Yen-Chi Chen, Shirley Ho, Rachel Mandelbaum, Neta A. Bahcall, Joel R. Brownstein, Peter E. Freeman, Christopher R. Genovese, Donald P. Schneider, and Larry Wasserman. Detecting effects of filaments on galaxy properties in the Sloan Digital Sky Survey III. *MNRAS*, 466(2):1880–1893, April 2017b. doi: 10.1093/mnras/stw3127.
- Jounghun Lee. A New Perspective on the Large-scale Tidal Effect on the Galaxy Luminosity and Morphology. *ApJ*, 867(1):36, November 2018. doi: 10.3847/1538-4357/aac376.
- C. Laigle, C. Pichon, S. Arnouts, H. J. McCracken, Y. Dubois, J. Devriendt, A. Slyz, D. Le Borgne, A. Benoit-Lévy, Ho Seong Hwang, O. Ilbert, K. Kraljic, N. Malavasi, Changbom Park, and D. Vibert. COSMOS2015 photometric redshifts probe the impact of filaments on galaxy properties. *MNRAS*, 474(4):5437–5458, March 2018. doi: 10.1093/mnras/stx3055.
- K. Kraljic, S. Arnouts, C. Pichon, C. Laigle, S. de la Torre, D. Vibert, C. Cadiou, Y. Dubois, M. Treyer, C. Schimd, S. Codis, V. de Lapparent, J. Devriendt, H. S. Hwang, D. Le Borgne, N. Malavasi, B. Milliard, M. Musso, D. Pogosyan, M. Alpaslan, J. Bland-Hawthorn, and A. H. Wright. Galaxy evolution in the metric of the cosmic web. *MNRAS*, 474(1):547–571, February 2018. doi: 10.1093/mnras/stx2638.
- Yen-Chi Chen, Shirley Ho, Jonathan Blazek, Siyu He, Rachel Mandelbaum, Peter Melchior, and Sukhdeep Singh. Detecting galaxy-filament alignments in the Sloan Digital Sky Survey III. *MNRAS*, 485(2):2492–2504, May 2019. doi: 10.1093/mnras/stz539.
- Katarina Kraljic, Christophe Pichon, Sandrine Codis, Clotilde Laigle, Romeel Davé, Yohan Dubois, Ho Seong Hwang, Dmitri Pogosyan, Stéphane Arnouts, Julien Devriendt, Marcello Musso, Sébastien Peirani, Adrienne Slyz, and Marie Treyer. The impact of the connectivity of the cosmic web on the physical properties of galaxies at its nodes. *MNRAS*, 491(3):4294–4309, January 2020. doi: 10.1093/mnras/stz3319.
- V. Bonjean, N. Aghanim, M. Douspis, N. Malavasi, and H. Tanimura. Filament profiles from WISExSCOS galaxies as probes of the impact of environmental effects. *A&A*, 638:A75, June 2020. doi: 10.1051/0004-6361/201937313.
- N. Winkel, A. Pasquali, K. Kraljic, R. Smith, A. Gallazzi, and T. M. Jackson. The imprint of cosmic web quenching on central galaxies. *MNRAS*, 505(4):4920–4934, August 2021. doi: 10.1093/mnras/stab1562.
- Nicola Malavasi, Mathieu Langer, Nabila Aghanim, Daniela Galárraga-Espinosa, and Céline Gouin. Relative effect of nodes and filaments of the cosmic web on the quenching of galaxies and the orientation of their spin. *A&A*, 658:A113, February 2022. doi: 10.1051/0004-6361/202141723.
- Pankaj C. Bhambhani, Ivan K. Baldry, Sarah Brough, Alexander D. Hill, M. A. Lara-Lopez, J. Loveday, and B. W. Holwerda. Red riding on hood:

- exploring how galaxy colour depends on environment. *MNRAS*, 522(3):4116–4131, July 2023. doi: 10.1093/mnras/stad1218.
- Anindita Nandi, Biswajit Pandey, and Prakash Sarkar. The correlations between galaxy properties in different environments of the cosmic web. *JCAP*, 2024(2):012, February 2024. doi: 10.1088/1475-7516/2024/02/012.
- Karl Pearson. Liii. on lines and planes of closest fit to systems of points in space. *Philosophical Magazine Series 1*, 2:559–572, 1901. URL <https://api.semanticscholar.org/CorpusID:125037489>.
- Chris Stoughton, Robert H. Lupton, Mariangela Bernardi, Michael R. Blanton, Scott Burles, Francisco J. Castander, A. J. Connolly, Daniel J. Eisenstein, Joshua A. Frieman, G. S. Hennessy, Robert B. Hindsley, Željko Ivezić, Stephen Kent, Peter Z. Kunszt, Brian C. Lee, Avery Meiksin, Jeffrey A. Munn, Heidi Jo Newberg, R. C. Nichol, Tom Nicinski, Jeffrey R. Pier, Gordon T. Richards, Michael W. Richmond, David J. Schlegel, J. Allyn Smith, Michael A. Strauss, Mark SubbaRao, Alexander S. Szalay, Aniruddha R. Thakar, Douglas L. Tucker, Daniel E. Vanden Berk, Brian Yanny, Jennifer K. Adelman, John E. Anderson, Jr., Scott F. Anderson, James Annis, Neta A. Bahcall, J. A. Bakken, Matthias Bartelmann, Steven Bastian, Amanda Bauer, Eileen Berman, Hans Böhringer, William N. Boroski, Steve Bracker, Charlie Briegel, John W. Briggs, J. Brinkmann, Robert Brunner, Larry Carey, Michael A. Carr, Bing Chen, Damian Christian, Patrick L. Colestock, J. H. Crocker, István Csabai, Paul C. Czarapata, Julianne Dalcanton, Arthur F. Davidsen, John Eric Davis, Walter Dehnen, Scott Dodelson, Mamoru Doi, Tom Dombek, Megan Donahue, Nancy Ellman, Brian R. Elms, Michael L. Evans, Laurent Eyer, Xiaohui Fan, Glenn R. Federwitz, Scott Friedman, Masataka Fukugita, Roy Gal, Bruce Gillespie, Karl Glazebrook, Jim Gray, Eva K. Grebel, Bruce Greenawalt, Gretchen Greene, James E. Gunn, Ernst de Haas, Zoltán Haiman, Merle Haldeman, Patrick B. Hall, Masaru Hamabe, Brad Hansen, Frederick H. Harris, Hugh Harris, Michael Harvanek, Suzanne L. Hawley, J. J. E. Hayes, Timothy M. Heckman, Amina Helmi, Arne Henden, Craig J. Hogan, David W. Hogg, Donald J. Holmgren, Jon Holtzman, Chih-Hao Huang, Charles Hull, Shin-Ichi Ichikawa, Takashi Ichikawa, David E. Johnston, Guinevere Kauffmann, Rita S. J. Kim, Tim Kimball, E. Kinney, Mark Klaene, S. J. Kleinman, Anatoly Klypin, G. R. Knapp, John Korienek, Julian Krolik, Richard G. Kron, Jurek Krzesiński, D. Q. Lamb, R. French Leger, Siriluk Limmongkol, Carl Lindenmeyer, Daniel C. Long, Craig Loomis, Jon Loveday, Bryan MacKinnon, Edward J. Mannery, P. M. Mantsch, Bruce Margon, Peregrine McGehee, Timothy A. McKay, Brian McLean, Kristen Menou, Aronne Merelli, H. J. Mo, David G. Monet, Osamu Nakamura, Vijay K. Narayanan, Thomas Nash, Eric H. Nielsen, Jr., Peter R. Newman, Atsuko Nitta, Michael Odenkirchen, Norio Okada, Sadanori Okamura, Jeremiah P. Ostriker, Russell Owen, A. George Pauls, John Peoples, R. S. Peterson, Donald Petravick, Adrian Pope, Ruth Pordes, Marc Postman, Angela Prosapio, Thomas R. Quinn, Ron Rechenmacher, Claudio H. Rivetta, Hans-Walter Rix, Constance M. Rockosi, Robert Rosner, Kurt Ruthmansdorfer, Dale Sandford, Donald P. Schneider, Ryan Scranton, Maki Sekiguchi, Gary Sergey, Ravi Sheth, Kazuhiro Shimasaku, Stephen Smee, Stephanie A. Snedden, Albert Stebbins, Christopher Stubbs, István Szapudi, Paula Szkody, Gyula P. Szokoly, Serge Tabachnik, Zlatan Tsvetanov, Alan Uomoto, Michael S. Vogeley, Wolfgang Voges, Patrick Waddell, René Walterbos, Shu-i. Wang, Masaru Watanabe, David H. Weinberg, Richard L. White, Simon D. M. White, Brian Willite, David Wolfe, Naoki Yasuda, Donald G. York, Idit Zehavi, and Wei Zheng. Sloan Digital Sky Survey: Early Data Release. *AJ*, 123(1): 485–548, January 2002. doi: 10.1086/324741.
- M. Einasto, L. J. Liivamägi, E. Saar, J. Einasto, E. Tempel, E. Tago, and V. J. Martínez. SDSS DR7 superclusters. Principal component analysis. *A&A*, 535:A36, November 2011. doi: 10.1051/0004-6361/201117529.
- Jonás Chaves-Montero and Andrew Hearin. Surrogate modelling the Baryonic Universe - I. The colour of star formation. *MNRAS*, 495(2): 2088–2104, June 2020. doi: 10.1093/mnras/staa1230.
- Andrés Balaguera-Antolínez, Antonio D. Montero-Dorta, and Ginevra Favole. Secondary halo bias through cosmic time. I. Scaling relations and the connection with the cosmic web. *A&A*, 685:A61, May 2024. doi: 10.1051/0004-6361/202348694.
- Planck Collaboration, N. Aghanim, Y. Akrami, M. Ashdown, J. Aumont, C. Baccigalupi, M. Ballardini, A. J. Banday, R. B. Barreiro, N. Bartolo, S. Basak, R. Battye, K. Benabed, J. P. Bernard, M. Bersanelli, P. Bielewicz, J. J. Bock, J. R. Bond, J. Borrill, F. R. Bouchet, F. Boulanger, M. Bucher, C. Burigana, R. C. Butler, E. Calabrese, J. F. Cardoso, J. Carron, A. Challinor, H. C. Chiang, J. Chluba, L. P. L. Colombo, C. Combet, D. Contreras, B. P. Crill, F. Cuttaia, P. de Bernardis, G. de Zotti, J. Delabrouille, J. M. Delouis, E. Di Valentino, J. M. Diego, O. Doré, M. Douspis, A. Ducout, X. Dupac, S. Dusini, G. Efstathiou, F. Elsner, T. A. Enßlin, H. K. Eriksen, Y. Fantaye, M. Farhang, J. Fergusson, R. Fernandez-Cobos, F. Finelli, F. Forastieri, M. Frailis, A. A. Fraisse, E. Franceschi, A. Frolov, S. Galeotta, S. Galli, K. Ganga, R. T. Génova-Santos, M. Gerbino, T. Ghosh, J. González-Nuevo, K. M. Górski, S. Gratton, A. Gruppuso, J. E. Gudmundsson, J. Hamann, W. Handley, F. K. Hansen, D. Herranz, S. R. Hildebrandt, E. Hivon, Z. Huang, A. H. Jaffe, W. C. Jones, A. Karakci, E. Keihänen, R. Keskitalo, K. Kiiveri, J. Kim, T. S. Kisner, L. Knox, N. Krachmalnicoff, M. Kunz, H. Kurki-Suonio, G. Lagache, J. M. Lamarre, A. Lasenby, M. Lattanzi, C. R. Lawrence, M. Le Jeune, P. Lemos, J. Lesgourgues, F. Levrier, A. Lewis, M. Liguori, P. B. Lilje, M. Lilley, V. Lindholm, M. López-Caniego, P. M. Lubin, Y. Z. Ma, J. F. Macías-Pérez, G. Maggio, D. Maino, N. Mandolesi, A. Mangilli, A. Marcos-Caballero, M. Maris, P. G. Martin, M. Martinelli, E. Martínez-González, S. Matarrese, N. Mauri, J. D. McEwen, P. R. Meinhold, A. Melchiorri, A. Mennella, M. Migliaccio, M. Millea, S. Mitra, M. A. Miville-Deschênes, D. Molinari, L. Montier, G. Morgante, A. Moss, P. Natoli, H. U. Nørgaard-Nielsen, L. Pagano, D. Paoletti, B. Partridge, G. Patanchon, H. V. Peiris, F. Perrotta, V. Pettorino, F. Piacentini, L. Polastri, G. Polenta, J. L. Puget, J. P. Rachen, M. Reinecke, M. Remazeilles, A. Renzi, G. Rocha, C. Rosset, G. Roudier, J. A. Rubiño-Martín, B. Ruiz-Granados, L. Salvati, M. Sandri, M. Savelainen, D. Scott, E. P. S. Shellard, C. Sirignano, G. Sirri, L. D. Spencer, R. Sunyaev, A. S. Suur-Uski, J. A. Tauber, D. Tavagnacco, M. Tenti, L. Toffolatti, M. Tomasi, T. Trombetti, L. Valenziano, J. Valiviita, B. Van Tent, L. Vibert, P. Vielva, F. Villa, N. Vittorio, B. D. Wandelt, I. K. Wehus, M. White, S. D. M. White, A. Zacchei, and A. Zonca. Planck 2018 results. VI. Cosmological parameters. *A&A*, 641:A6, September 2020. doi: 10.1051/0004-6361/201833910.
- Andrés Almeida, Scott F. Anderson, Maria Argudo-Fernández, Carles Badenes, Kat Barger, Jorge K. Barrera-Ballesteros, Chad F. Bender, Erika Benitez, Felipe Besser, Jonathan C. Bird, Dmitry Bizyaev, Michael R. Blanton, John Bochanski, Jo Bovy, William Nielsen Brandt, Joel R. Brownstein, Johannes Buchner, Esra Bulbul, Joseph N. Burchett, Mariana Cano Díaz, Joleen K. Carlberg, Andrew R. Casey, Vedant Chandra, Brian Cherinka, Cristina Chiappini, Abigail A. Coker, Johan Comparat, Charlie Conroy, Gabriella Contardo, Arlin Cortes, Kevin Covey, Jeffrey D. Crane, Katia Cunha, Collin Dabbieri, James W. Davidson, Megan C. Davis, Anna Barbara de Andrade Queiroz, Nathan De Lee, José Eduardo Méndez Delgado, Sebastian Demasi, Francesco Di Mille, John Donor, Peter Dow, Tom Dwelly, Mike Eracleous, Jamey Eriksen, Xiaohui Fan, Emily Farr, Sara Frederick, Logan Fries, Peter Frinchaboy, Boris T. Gänsicke, Junqiang Ge, Consuelo González Ávila, Katie Grabowski, Catherine Grier, Guillaume Guiglion, Pramod Gupta, Patrick Hall, Keith Hawkins, Christian R. Hayes, J. J. Hermes, Lorena Hernández-García, David W. Hogg, Jon A. Holtzman, Hector Javier Ibarra-Medel, Alexander Ji, Paula Jofre, Jennifer A. Johnson, Amy M. Jones, Karen Kinemuchi, Matthias Kluge, Anton Koekemoer, Juna A. Kollmeier, Marina Kounkel, Dhanesh Krishnarao, Mirko Krumpke,

- Ivan Lacerna, Paulo Jakson Assuncao Lago, Chervin Laporte, Chao Liu, Ang Liu, Xin Liu, Alexandre Roman Lopes, Matin Macktoobian, Steven R. Majewski, Viktor Malanushenko, Dan Maoz, Thomas Masseron, Karen L. Masters, Gal Matijevic, Aidan McBride, Ilija Medan, Andrea Merloni, Sean Morrison, Natalie Myers, Szabolcs Mészáros, C. Alenka Negrete, David L. Nidever, Christian Nitschelm, Daniel Oravetz, Audrey Oravetz, Kaike Pan, Yingjie Peng, Marc H. Pinsonneault, Rick Pogge, Dan Qiu, Solange V. Ramirez, Hans-Walter Rix, Daniela Fernández Rosso, Jessie Runnoe, Mara Salvato, Sebastian F. Sanchez, Felipe A. Santana, Andrew Saydjari, Conor Sayres, Kevin C. Schlafman, Donald P. Schneider, Axel Schwobe, Javier Serna, Yue Shen, Jennifer Sobeck, Ying-Yi Song, Diogo Souto, Taylor Spoo, Keivan G. Stassun, Matthias Steinmetz, Ilya Straumit, Guy Stringfellow, José Sánchez-Gallego, Manuchehr Taghizadeh-Popp, Jamie Tayar, Ani Thakar, Patricia B. Tissera, Andrew Tkachenko, Hector Hernandez Toledo, Benny Trakhtenbrot, José G. Fernández-Trincado, Nicholas Troup, Jonathan R. Trump, Sarah Tuttle, Natalie Ulloa, Jose Antonio Vazquez-Mata, Pablo Vera Alfaro, Sandro Villanova, Stefanie Wachter, Anne-Marie Weijmans, Adam Wheeler, John Wilson, Leigh Wojno, Julien Wolf, Xiang-Xiang Xue, Jason E. Ybarra, Eleonora Zari, and Gail Zasowski. The Eighteenth Data Release of the Sloan Digital Sky Surveys: Targeting and First Spectra from SDSS-V. *ApJS*, 267(2):44, August 2023. doi: 10.3847/1538-4365/acda98.
- Kazuhiro Shimasaku, Masataka Fukugita, Mamoru Doi, Masaru Hamabe, Takashi Ichikawa, Sadanori Okamura, Maki Sekiguchi, Naoki Yasuda, Jon Brinkmann, István Csabai, Shin-Ichi Ichikawa, Zeljko Ivezić, Peter Z. Kunszt, Donald P. Schneider, Gyula P. Szokoly, Masaru Watanabe, and Donald G. York. Statistical Properties of Bright Galaxies in the Sloan Digital Sky Survey Photometric System. *AJ*, 122(3):1238–1250, September 2001. doi: 10.1086/322094.
- Charlie Conroy, James E. Gunn, and Martin White. The Propagation of Uncertainties in Stellar Population Synthesis Modeling. I. The Relevance of Uncertain Aspects of Stellar Evolution and the Initial Mass Function to the Derived Physical Properties of Galaxies. *ApJ*, 699(1):486–506, July 2009. doi: 10.1088/0004-637X/699/1/486.
- Martin Asplund, Nicolas Grevesse, A. Jacques Sauval, and Pat Scott. The Chemical Composition of the Sun. *Annual Review of Astronomy and Astrophysics*, 47(1):481–522, September 2009. doi: 10.1146/annurev.astro.46.060407.145222.
- J. Brinchmann, S. Charlot, S. D. M. White, C. Tremonti, G. Kauffmann, T. Heckman, and J. Brinkmann. The physical properties of star-forming galaxies in the low-redshift Universe. *MNRAS*, 351(4):1151–1179, July 2004. doi: 10.1111/j.1365-2966.2004.07881.x.
- G. Bruzual A. Spectral evolution of galaxies. I. Early-type systems. *ApJ*, 273:105–127, October 1983. doi: 10.1086/161352.
- Michael L. Balogh, Simon L. Morris, H. K. C. Yee, R. G. Carlberg, and Erica Ellingson. Differential Galaxy Evolution in Cluster and Field Galaxies at  $z < 0.3$ . *ApJ*, 527(1):54–79, December 1999. doi: 10.1086/308056.
- Oliver Hahn, C. Marcella Carollo, Cristiano Porciani, and Avishai Dekel. The evolution of dark matter halo properties in clusters, filaments, sheets and voids. *MNRAS*, 381(1):41–51, October 2007. doi: 10.1111/j.1365-2966.2007.12249.x.
- J. E. Forero-Romero, Y. Hoffman, S. Gottlöber, A. Klypin, and G. Yepes. A dynamical classification of the cosmic web. *MNRAS*, 396(3):1815–1824, July 2009. doi: 10.1111/j.1365-2966.2009.14885.x.
- C. Spearman. The american journal of psychology. *Am. J. Psychol.*, 15:88, 1904.
- C. E. Shannon. A mathematical theory of communication. *The Bell System Technical Journal*, 27(3):379–423, 1948. doi: 10.1002/j.1538-7305.1948.tb01338.x.
- Alexander Strehl and Joydeep Ghosh. Cluster ensembles — a knowledge reuse framework for combining multiple partitions. *J. Mach. Learn. Res.*, 3:583–617, 2002. URL <https://api.semanticscholar.org/CorpusID:3068944>.
- Biswajit Pandey, Gauri Kulkarni, Somnath Bharadwaj, and Tarun Souradeep. The size of the longest filament in the luminous red galaxy distribution. *MNRAS*, 411(1):332–336, February 2011. doi: 10.1111/j.1365-2966.2010.17686.x.
- Prakash Sarkar, Biswajit Pandey, and Suman Sarkar. The maximum extent of the filaments and sheets in the cosmic web: an analysis of the SDSS DR17. *MNRAS*, 519(3):3227–3236, March 2023. doi: 10.1093/mnras/stac3722.
- F. Nicastro, J. Kaastra, Y. Krongold, S. Borgani, E. Branchini, R. Cen, M. Dadina, C. W. Danforth, M. Elvis, F. Fiore, A. Gupta, S. Mathur, D. Mayya, F. Paerels, L. Piro, D. Rosa-Gonzalez, J. Schaye, J. M. Shull, J. Torres-Zafra, N. Wijers, and L. Zappacosta. Observations of the missing baryons in the warm-hot intergalactic medium. *Nature*, 558(7710):406–409, June 2018. doi: 10.1038/s41586-018-0204-1.
- Shihong Liao and Liang Gao. Impact of filaments on galaxy formation in their residing dark matter haloes. *MNRAS*, 485(1):464–473, May 2019. doi: 10.1093/mnras/stz441.
- Punyakoti Ganeshaiah Veena, Marius Cautun, Rien van de Weygaert, Elmo Tempel, Bernard J. T. Jones, Steven Rieder, and Carlos S. Frenk. The Cosmic Ballet: spin and shape alignments of haloes in the cosmic web. *MNRAS*, 481(1):414–438, November 2018. doi: 10.1093/mnras/sty2270.
- N. Malavasi, S. Arnouts, D. Vibert, S. de la Torre, T. Moutard, C. Pichon, I. Davidzon, K. Kraljic, M. Bolzonella, L. Guzzo, B. Garilli, M. Scoddegio, B. R. Granett, U. Abbas, C. Adami, D. Bottini, A. Cappi, O. Cucciati, P. Franzetti, A. Fritz, A. Iovino, J. Krywult, V. Le Brun, O. Le Fèvre, D. Maccagni, K. Małek, F. Marulli, M. Polletta, A. Pollo, L. Tasca, R. Tojeiro, D. Vergani, A. Zanichelli, J. Bel, E. Branchini, J. Coupon, G. De Lucia, Y. Dubois, A. Hawken, O. Ilbert, C. Laigle, L. Moscardini, T. Sousbie, M. Treyer, and G. Zamorani. The VIMOS Public Extragalactic Redshift Survey (VIPERS): galaxy segregation inside filaments at  $z \approx 0.7$ . *MNRAS*, 465(4):3817–3822, March 2017. doi: 10.1093/mnras/stw2864.
- Hyunmi Song, Clotilde Laigle, Ho Seong Hwang, Julien Devriendt, Yohan Dubois, Katarina Kraljic, Christophe Pichon, Adrienne Slyz, and Rory Smith. Beyond halo mass: quenching galaxy mass assembly at the edge of filaments. *MNRAS*, 501(3):4635–4656, March 2021. doi: 10.1093/mnras/staa3981.
- Sachin Kotecha, Charlotte Welker, Zihan Zhou, James Wadsley, Katarina Kraljic, Jenny Sorce, Elena Rasia, Ian Roberts, Meghan Gray, Gustavo Yepes, and Weiguang Cui. Cosmic filaments delay quenching inside clusters. *MNRAS*, 512(1):926–944, May 2022. doi: 10.1093/mnras/stac300.
- Wes McKinney. *Python for Data Analysis*. O'Reilly Media, Inc., 2010.
- Charles R. Harris, K. Jarrod Millman, Stéfan J. van der Walt, Ralf Gommers, Pauli Virtanen, David Cournapeau, Eric Wieser, Julian Taylor, Sebastian Berg, Nathaniel J. Smith, Robert Kern, Matti Picus, Stephan Hoyer, Marten H. van Kerkwijk, Matthew Brett, Allan Haldane, Jaime Fernández del Río, Mark Wiebe, Pearu Peterson, Pierre Gérard-Marchant, Kevin Sheppard, Tyler Reddy, Warren Weckesser, Hameer Abbasi, Christoph Gohlke, and Travis E. Oliphant. Array programming with NumPy. *Nature*, 585(7825):357–362, September 2020. doi: 10.1038/s41586-020-2649-2.
- Pauli Virtanen, Ralf Gommers, Travis E. Oliphant, Matt Haberland, Tyler Reddy, David Cournapeau, Evgeni Burovski, Pearu Peterson, Warren Weckesser, Jonathan Bright, Stéfan J. van der Walt, Matthew Brett, Joshua Wilson, K. Jarrod Millman, Nikolay Mayorov, Andrew R. J. Nelson,

Eric Jones, Robert Kern, Eric Larson, C. J. Carey, İlhan Polat, Yu Feng, Eric W. Moore, Jake VanderPlas, Denis Laxalde, Josef Perktold, Robert Cimrman, Ian Henriksen, E. A. Quintero, Charles R. Harris, Anne M. Archibald, Antônio H. Ribeiro, Fabian Pedregosa, Paul van Mulbregt, and SciPy 1.0 Contributors. SciPy 1.0: fundamental algorithms for scientific computing in Python. *Nature Methods*, 17:261–272, February 2020. doi: 10.1038/s41592-019-0686-2.

John D. Hunter. Matplotlib: A 2D Graphics Environment. *Computing in Science and Engineering*, 9(3):90–95, May 2007. doi: 10.1109/MCSE.2007.55.